

Design and Synthesis of EZH2-Based PROTACs to Degrade the PRC2 Complex for Targeting the Noncatalytic Activity of EZH2

Zhihao Liu,^{||} Xi Hu,^{||} Qiwei Wang, Xiuli Wu, Qiangsheng Zhang, Wei Wei, Xingping Su, Hualong He, Shuyan Zhou, Rong Hu, Tinghong Ye, Yongxia Zhu, Ningyu Wang,* and Luoting Yu*Cite This: *J. Med. Chem.* 2021, 64, 2829–2848

Read Online

ACCESS |



Metrics & More

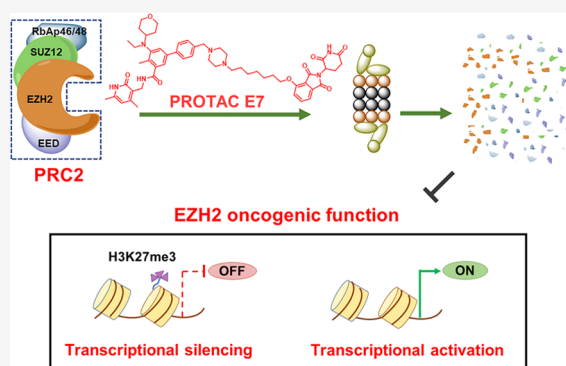


Article Recommendations



Supporting Information

ABSTRACT: EZH2 mediates both PRC2-dependent gene silencing via catalyzing H3K27me3 and PRC2-independent transcriptional activation in various cancers. Given its oncogenic role in cancers, EZH2 has constituted a compelling target for anticancer therapy. However, current EZH2 inhibitors only target its methyltransferase activity to downregulate H3K27me3 levels and show limited efficacy because of inadequate suppression of the EZH2 oncogenic activity. Therefore, therapeutic strategies to completely block the oncogenic activity of EZH2 are urgently needed. Herein, we report a series of EZH2-targeted proteolysis targeting chimeras (PROTACs) that induce proteasomal degradation of PRC2 components, including EZH2, EED, SUZ12, and RbAp48. Preliminary assessment identified E7 as the most active PROTAC molecule, which decreased PRC2 subunits and H3K27me2/3 levels in various cancer cells. Furthermore, E7 strongly inhibited transcriptional silencing mediated by EZH2 dependent on PRC2 and transcriptional activation mediated by EZH2 independent of PRC2, showing significant antiproliferative activities against cancer cell lines dependent on the enzymatic and nonenzymatic activities of EZH2.



INTRODUCTION

Polycomb repressive complex 2 (PRC2) is a conserved multicomponent transcriptional repressive complex with histone methyltransferase activity that catalyzes the dimethylation and trimethylation of lysine residue 27 on histone H3 (H3K27me2/3) and silences target genes that are involved in fundamental cellular processes by facilitating chromatin compaction.^{1–4} The mammalian PRC2 complex mainly possesses four key subunits: enhancer of the zeste homolog 1/2 (EZH1/2), embryonic ectoderm development (EED), suppressor of the zeste 12 protein homolog (SUZ12), and retinoblastoma (Rb)-associated proteins 46/48 (RbAp46 or RBBP7/RbAp48 or RBBP4).^{1,5} Overactivation of the PRC2 complex induces the occurrence of malignant tumors by silencing tumor suppressor genes.⁶

As the core catalytic subunit of PRC2, EZH2 is frequently overexpressed in many cancer types including breast, prostate, lung, and ovarian cancers, and overexpression of EZH2 is implicated in tumorigenesis and poor prognosis in several cancers.^{7–14} In germinal center B-cell (GCB) diffuse large-cell B-cell lymphomas (DLBCLs), EZH2 point mutations at Y641 (Y641F, Y641N, Y641S, Y641C, and Y641H) occur in about 22% cases, and these Y641 mutations are also identified in 7–12% of follicular lymphomas.^{15–17} In addition, A677 and A687 mutations in EZH2 have also been found in non-Hodgkin's lymphomas (NHLs).^{18,19} All of these mutations confer gain of

function of enzyme activity, resulting in hypertrimethylated H3K27 status and promotion of tumorigenesis in several types of tumors. In view of the important role of dysfunctional EZH2 in tumorigenesis, the development of EZH2-specific inhibitors has been an important research area.⁶ Several S-adenosyl-L-methionine (SAM)-competitive compounds that target EZH2, including GSK126,²⁰ EPZ6438,^{21,22} PF-06821497,²³ and CPI-1205,²⁴ are currently in clinical trials, and these compounds have demonstrated efficacies in treating hematological malignancies, sarcomas, and malignant rhabdoid tumors. Recently, the U.S. FDA has granted accelerated approval of TAZVERIK (tazemetostat, EPZ6438) for the treatment of patients with metastatic or locally advanced epithelioid sarcoma.²⁵

However, the clinical efficacy of EZH2 inhibitors remains unsatisfactory and is limited to certain cancers.²⁶ As a multifunctional protein, EZH2 not only mediates gene silencing via recruitment of the PRC2 complex to catalyze H3K27me3 but also mediates transcriptional activation

Received: December 24, 2020

Published: February 19, 2021



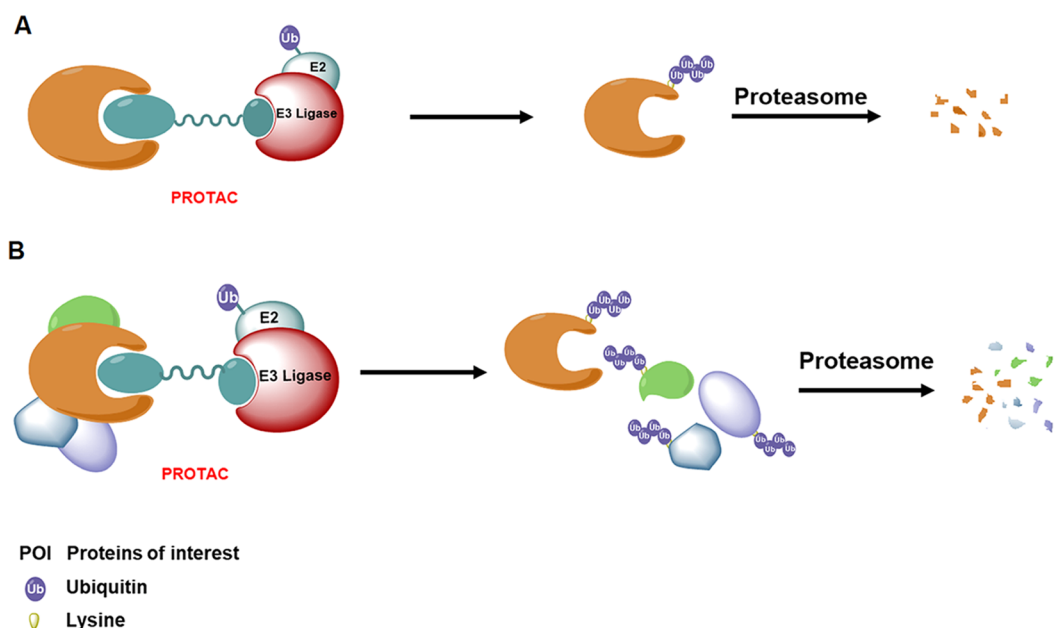


Figure 1. Schematic of PROTAC inducing POI degradation (A). Proposed model for PROTAC inducing degradation of a protein complex (B).

independent of EZH2/PRC2 catalytic activity in some cancers.^{27–29} In estrogen receptor (ER)-negative basal-like breast cancer cells, EZH2 interacts with RelA and RelB and induces continuous activation of the NF- κ B downstream signaling pathway independent of its catalytic activity.³⁰ In castration-resistant prostate cancer (CRPC), the PI3K-Akt pathway mediates the phosphorylation of EZH2 at Ser21 and switches its function from a polycomb repressor to a PRC2-independent transcriptional coactivator of AR.^{31,32} Kim et al.³³ showed that the growth and survival of SWI/SNF mutant tumors rely on both the catalytic and noncatalytic activities of EZH2, and the EZH2 inhibitor GSK126 only showed limited efficacy in SWI/SNF-mutant cancer cells. Therefore, EZH2 inhibitors that target EZH2 methyltransferase activity are only efficacious in a few cancers because of their inadequate suppression of EZH2 oncogenic activity, and therapeutic strategies to completely block the oncogenic functions of EZH2 are urgently needed.

Regulation of EZH2 homeostasis may be an effective therapeutic approach to treat cancers dependent on and independent of EZH2/PRC2 catalytic activity. Hydrophobic tagging (HyT) and proteolysis targeting chimeras (PROTACs) are practical and feasible approaches for regulation of protein homeostasis via degradation of the target protein.³⁴ HyT technology uses bifunctional molecules to induce protein degradation by appending a hydrophobic tag such as adamantane on the target protein to mimic protein misfolding.³⁵ Recently, Ma et al.³⁶ reported a first-in-class EZH2 selective degrader MS1943 based on HyT. MS1943 effectively reduced EZH2 and SUZ12 protein levels without affecting EED protein levels in triple-negative breast cancer (TNBC) cells and showed significant antiproliferative activities in multiple TNBC cells that are insensitive to EZH2 inhibitors.

PROTACs apply a linker to concatenate a ligand of E3 ubiquitin ligase and a ligand for a protein of interest (POI) and function by recruiting the E3 ubiquitin ligase close to the POI to promote consequent degradation of the POI (Figure 1A).^{37–39} Almost all reported PROTACs just induce the degradation of their direct interactive proteins, while few

studies have mentioned the possibility of PROTACs degrading their indirect interactive proteins, for instance, the components of a protein complex. Actually, Hsu et al.⁴⁰ and Potjewyd et al.⁴¹ recently described the discovery of EED-targeted PROTACs that indeed led to the degradation of multiple components of the PRC2 complex such as EED, EZH2, and SUZ12 although the in-depth mechanism was not fully interpreted. Since the PROTAC molecule plays a binder role in drawing the E3 ubiquitin ligase close to the POI, we hypothesize that if the POI is capable of forming a protein complex with other proteins, then the PROTAC molecule could also induce the degradation of other components of the complex by drawing the E3 ubiquitin ligase close to the complex or downregulating the stability of these proteins due to the inability to form a protein complex (Figure 1B).

Based on the above assumptions, we hypothesized that EZH2-targeted PROTACs, like EED-targeted PROTACs, could induce the depletion of the PRC2 complex as well, leading to inhibition of both the catalytic and noncatalytic functions of EZH2 and providing extensive anticancer activity. In this study, we designed and synthesized the EZH2-targeted PROTACs to investigate their ability and specific mechanism to degrade the PRC2 complex and examined whether the EZH2-targeted PROTACs could inhibit both the catalytic and noncatalytic functions of EZH2 and exhibit more extensive antitumor effects.

RESULTS AND DISCUSSION

The degradation efficiency of a PROTAC molecule typically hinges on the spatial orientation of the POI and the E3 ligase upon PROTAC conjugation, the affinity of the PROTAC with the POI, and the fitness of the connectome part.^{42–45} To identify a suitable modification site on an EZH2 inhibitor that can join to a linker moiety without a significant loss in potency, we first analyzed the binding mode between the EZH2 inhibitor GSK126 and the PRC2 complex with a reported cocrystal structure (PDB: 5WG6)⁴⁶ and found that the piperazinyl fragment in GSK126 extended into the solvent region and did not touch the other subunits of the PRC2

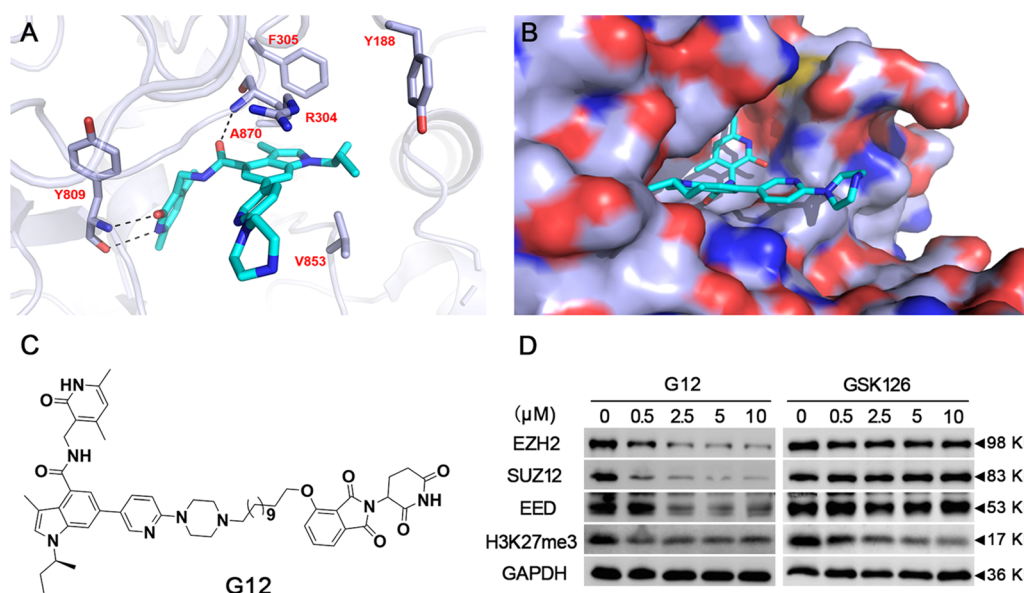
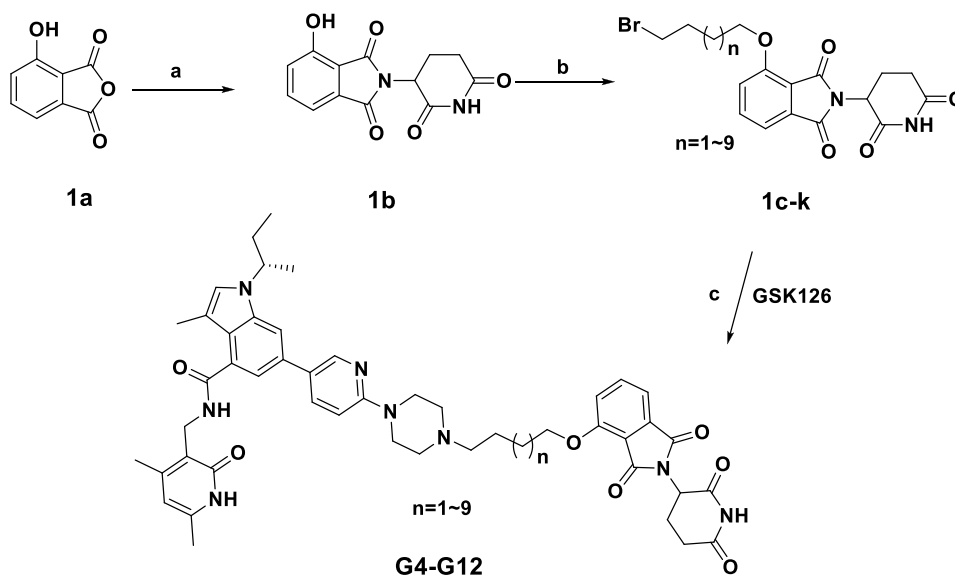


Figure 2. Design and proof-of-concept experiments for degrading the PRC2 complex of EZH2-targeted PROTACs. (A) Structure of GSK126 bound to PRC2 (PDB: 5WG6). (B) Spatial orientation of GSK126 toward the solvent region (PDB: 5WG6). (C) Structure of G12. (D) Levels of PRC2 subunits and H3K27me3 after treatment with various concentrations of G12 or GSK126, 72 h.

Scheme 1. Syntheses of Compounds G4–G12^a



^aReagents and conditions: (a) Ac₂O, 3-aminopiperidine-2,6-dione, 140 °C, 6 h, 71%; (b) DMF, dibromoalkane, *N,N*-diisopropylethylamine (DIPEA), 85–100 °C, 3–6 h, 34–63%; (c) GSK126, NaHCO₃, 85–100 °C, 3–8 h, 14–41%.

complex (Figure 2A,B). We also found that the orientation of the morpholine moiety in EPZ6438 also extended into the solvent region after the molecular superposition of EPZ6438 and GSK126. 4-Hydroxythalidomide, a well-studied ligand of the cereblon (CRBN) component of E3 ligase, was used as the ligand to conjugate to the piperazine N-atom in GSK126 through a long alkyl linker (G12, Figure 2C). We then investigated the potential degradation ability of G12 to PRC2 subunits including EZH2. GSK126 only inhibited H3K27 trimethylation without detectable effects on the PRC2 subunit expression (Figure 2D). By contrast, G12 dose-dependently decreased both EZH2 and H3K27me3 levels in the DLBCL cell line WSU-DLCL-2. Intriguingly, G12 also demonstrated

strong degradation efficiency against EED and SUZ12, implying the possibility of degrading multiple subunits of a complex by a specific subunit-targeted PROTAC.

Inspired by the preliminary proof-of-concept experiments, we conducted an in-depth structure–activity relationship study to optimize the PROTAC molecules. Various alkyl linkers with different lengths were incorporated to connect selective EZH2 inhibitors, such as EPZ6438 or GSK126, with the CRBN ligand 4-hydroxythalidomide to investigate their degradation efficiency against PRC2 subunits. The general synthetic route of compounds G4–G12 is illustrated in Scheme 1. Racemic hydroxythalidomide (1b) was obtained through the ammonolysis reaction of 4-hydroxyisobenzofuran-1,3-dione and

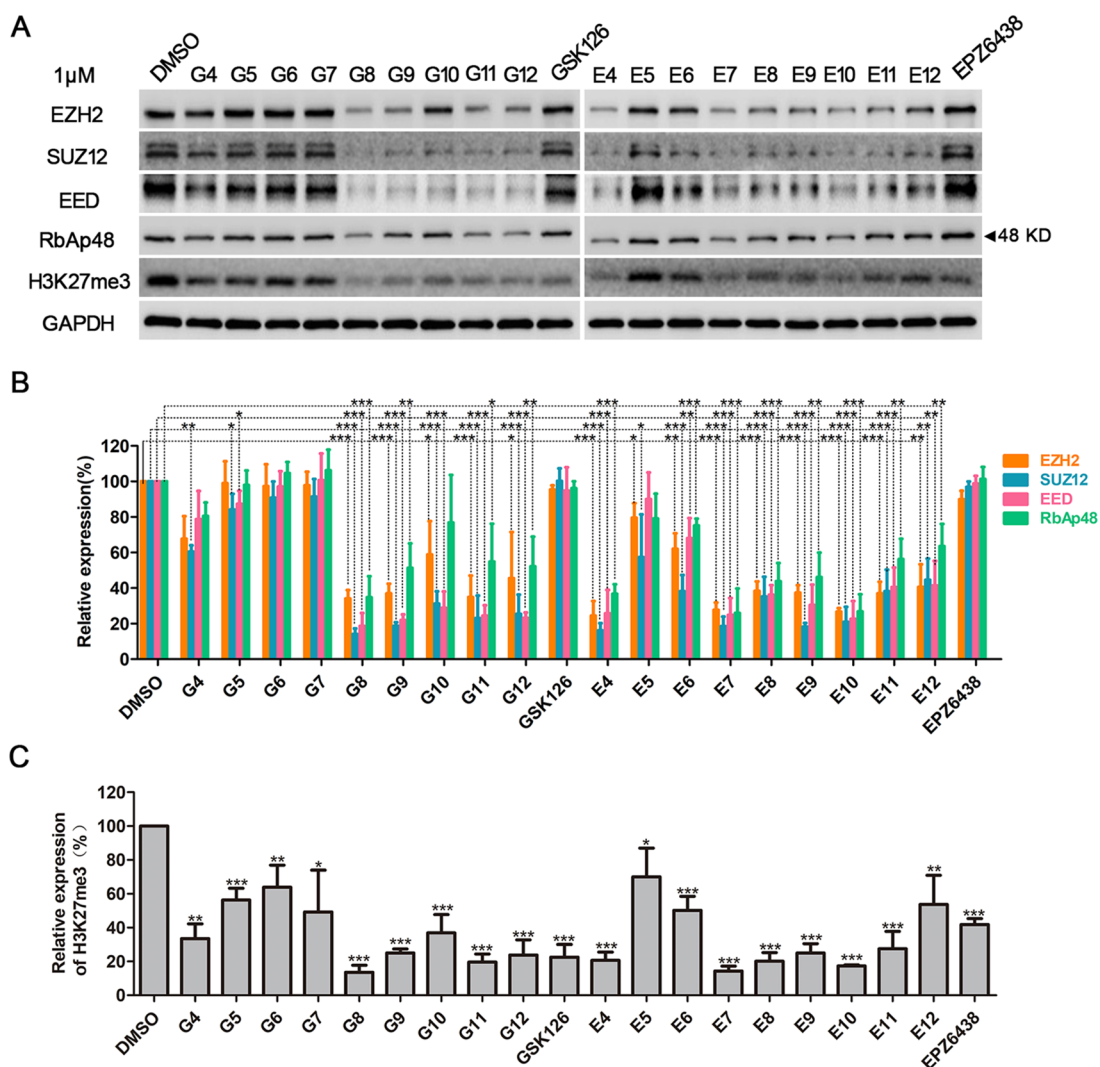


Figure 3. PROTACs degrade PRC2 subunits and decrease H3K27me3 levels. (A) PRC2 subunits and H3K27me3 levels in WSU-DLCL-2 cells treated with 1 μ M PROTACs, GSK126, or EPZ6438 for 48 h were analyzed. A representative western blot (WB) of three experiments is presented. GAPDH served as the internal control. (B) Quantitative results of the EZH2, SUZ12, EED, and RbAp48 levels detected by western blot. (C) Quantitative results of H3K27me3 levels detected by western blot. Protein levels were quantified by densitometry analysis using Image J and normalized against GAPDH levels. Data are expressed as mean \pm SD from three independent experiments, * p < 0.05, ** p < 0.01, and *** p < 0.001, compared with the DMSO-treated group by the t -test.

1c–k to obtain PROTAC molecules G4–G12 based on GSK126 (14–41% yield).

Scheme 2 shows the synthetic route for compounds E4–E12. The key intermediate of EPZ6438-based PROTACs 2g was accomplished according to a previously published method for the preparation of EPZ6438.²¹ Briefly, E4–E12 were synthesized starting from methyl 5-bromo-2-methyl-3-nitrobenzoate (2a) with reduction, two steps of reductive amination, hydrolysis, and amide condensation to afford the intermediate 2f. Suzuki coupling of 2f with aryl boronate esters using Pd(dppf)Cl₂ and cesium carbonate and subsequent deprotection afforded 2g. PROTACs E4–E12 with varying linker lengths were obtained by SN₂ reactions between 1c–k and 2g.

The title compounds were evaluated for their EZH2 inhibitory potency in an Alpha-Screen assay, and EPZ6438 and GSK126 were used as positive controls. As shown in Table 1, PROTACs G4–G12 and E4–E12 showed similar overall inhibition properties with nanomolar IC₅₀ against EZH2.

Compounds E4–E8 and G4–G8 with a linker length of 4–8 carbon atoms demonstrated comparable inhibitory activity against EZH2 to that of the positive control EPZ6438 and GSK126. When the length of linkers was further extended to 9–12 carbon atoms (E9–E12 and G9–G12), the inhibitory activities against EZH2 were 5–80 times less potent than GSK126. In general, E7 showed the highest potency (IC₅₀ = 2.7 nM) for inhibiting the EZH2 methyltransferase activity and exhibited >66-fold selectivity for EZH2 over its paralog EZH1 (EZH1 IC₅₀ = 179.0 nM, Table S1).

We then evaluated the degradation efficiency of all EZH2-targeted PROTACs against EZH2, EED, SUZ12, and RbAp48 upon treatment with title compounds in a fixed concentration and time (1 μ M, 48 h) in the WSU-DLCL-2 cancer cell line (Figures 3A,B and S1). As expected, EPZ6438 and GSK126 did not alter the levels of all PRC2 subunits. Among the G-series PROTACs, G4–G7 with a linker length of 4–7 carbon atoms showed poor degradation abilities against PRC2 subunits, while PROTACs with a linker length of 8–12

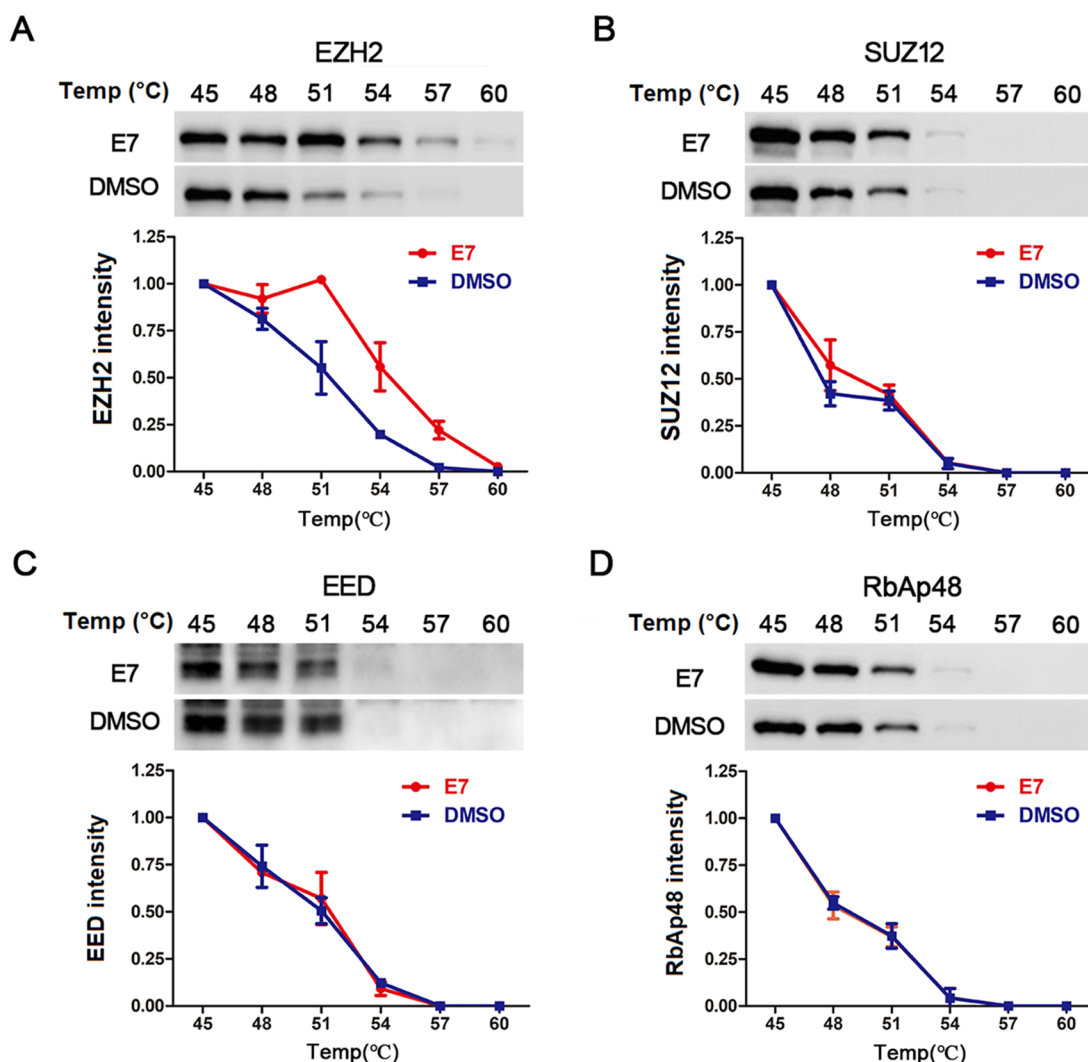


Figure 4. Binding of EZH2 (A), SUZ12 (B), EED (C), and RbAp48 (D) to E7 in WSU-DLCL-2 cells was detected by the thermo shift assay. Bands in immunoblotting were quantified by densitometry analysis using Image J. WSU-DLCL-2 cells were pretreated with MG-132 (5 μ M for 1 h) before treatment with E7 (60 μ M for 2 h). Cell lysates were examined by western blot. Data are expressed as mean \pm SD from three independent experiments.

carbon atoms (G8–G12) demonstrated significant degradation efficiency against all PRC2 subunits to different extents. The degradation of SUZ12 and EED was much more efficient than that of the primary target EZH2 across this series. Among EZH2-targeted PROTACs based on EPZ6438, E4 with a 4-C linker demonstrated a strong degradation efficiency against EZH2, EED, SUZ12, and RbAp48. A possible explanation for this phenomenon may be that E4 with a shorter linker could induce an alternative ternary complex conformation between EZH2 and CRBN, which is different from other EZH2-PROTACs, as the previously reported BRD4-PROTACs.⁴⁷ E5 and E6 also degraded PRC2 subunits to some extent, but their degradation abilities were significantly weaker than that of E4. E7–E12 significantly degraded PRC2 subunits, but the degradation abilities became weaker as the length of the linker was prolonged from 7 to 12 carbon atoms.

We also investigated the effects of synthesized EZH2-targeted PROTACs on H3K27me3 levels. We treated WSU-DLCL-2 cells with PROTACs, GSK126, or EPZ6438 at 1 μ M for 48 h to monitor H3K27me3 levels by western blot. As shown in Figure 3A,C, the trend of decreasing H3K27me3

levels was consistent with the decreasing level of PRC2 complex subunits after PROTAC treatment. PROTACs that induced the degradation of PRC2 subunits (G8–G12, E4, E7–E11) also significantly decreased H3K27me3 levels in WSU-DLCL-2 cancer cells. Among the CRBN-recruiting PROTACs, E7 demonstrated the best degradation efficacies against all PRC2 subunits (EZH2 72%, SUZ12 81%, EED 75%, RbAp48 74%) and a maximum decrease in H3K27me3 levels (reduced by 83%) at 1 μ M for 48 h. Hence, E7 was finally selected for further study.

Cellular thermal shift assay is a technology for evaluating ligand binding to target proteins in cells that uses the shift in protein thermal stability caused by drug binding to directly monitor target protein–drug interactions in cells.⁴⁸ To investigate which subunit of PRC2 could bind to E7, we conducted thermal shift assays in WSU-DLCL-2 cells. E7 increased the thermal stability of EZH2, with a temperature shift of approximately 5 $^{\circ}$ C, indicating a direct binding of E7 and the EZH2 protein (Figure 4A). However, E7 did not shift the thermal denaturation curves of EED, SUZ12, and RbAp48, suggesting that E7 might not directly bind to SUZ12, EED,

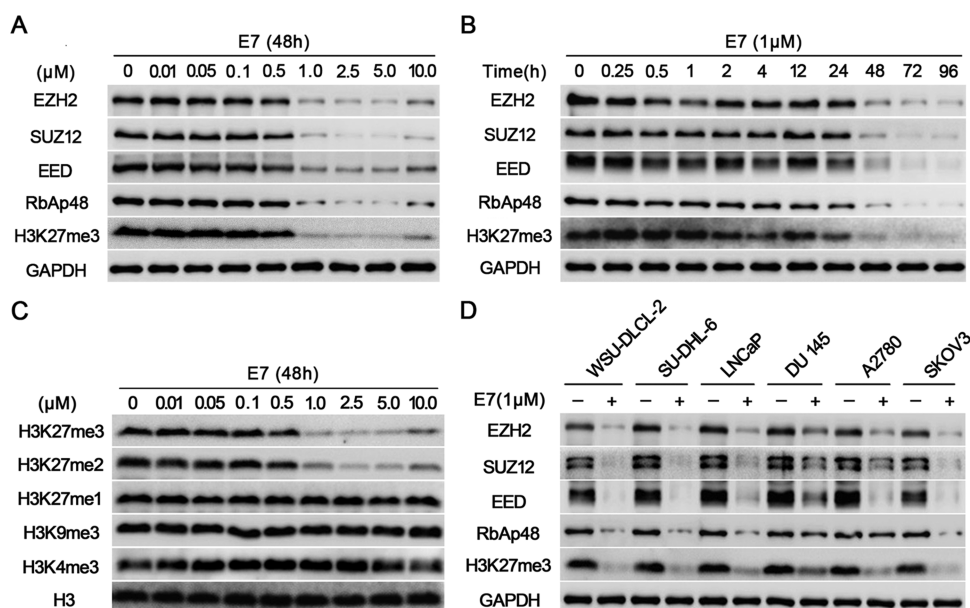


Figure 5. E7 effectively degrades PRC2 subunits and specifically inhibits PRC2. (A) Decrease in PRC2 subunits and H3K27me3 levels is dependent on E7 concentrations. WSU-DLCL-2 cells were incubated with E7 for 48 h at indicated concentrations. (B) Time course of PRC2 subunits' degradation and H3K27me3 decrease by E7 (1 μM) in WSU-DLCL2 cells. (C) Effects of E7 on histone H3 methylation in WSU-DLCL-2 cells were detected by western blot. (D) Western blot analysis of PRC2 subunits and H3K27me3 following treatment of E7 (1 μM for 48 h) in DLBCL (WSU-DLCL-2, Pfeiffer), prostate cancer (LNCaP, DU 145), and ovarian cancer (A2780, SKOV3) cell lines.

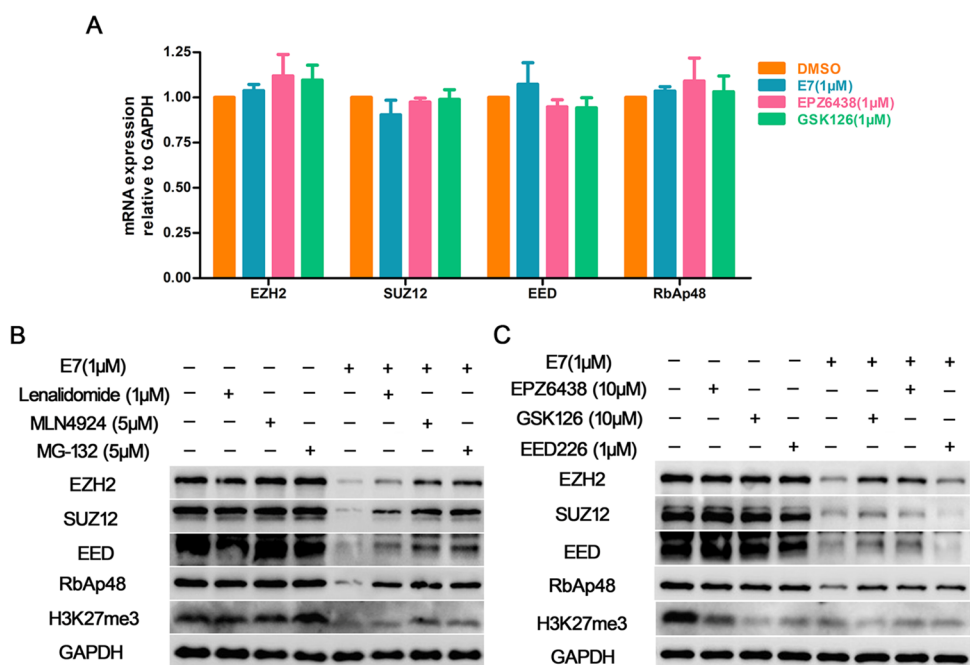
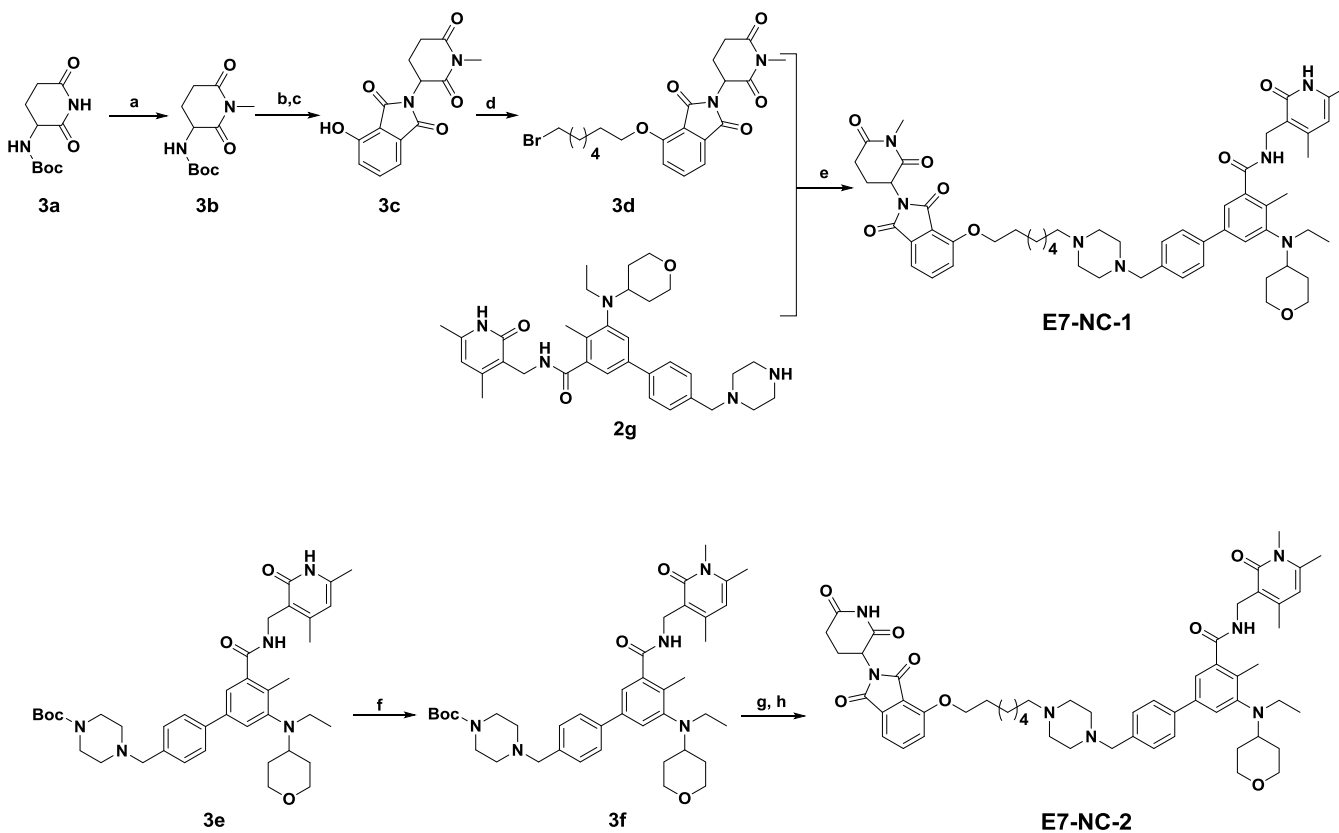


Figure 6. E7 induces the degradation of the PRC2 complex via the ubiquitin-proteasomal pathway. (A) RT-qPCR analysis of the mRNA levels of PRC2 subunits in WSU-DLCL-2 cells following treatment with E7 (1 μM for 48 h). The mRNA levels of PRC2 components were normalized to levels in the DMSO-treated group. Error bars represent mean \pm SD analyzed by the *t*-test. (B) WSU-DLCL-2 cells were pretreated with lenalidomide or MLN4924/MG-132 for 4 h, followed by treatment with E7 for an additional 48 h. (C) Competitive effects of EZH2 or EED inhibitors in WSU-DLCL-2 cells on E7 were determined by western blot. Cells were treated with indicated compounds for 48 h.

and RbAp48 protein (Figure 4B–D). Overall, these data confirmed that our bivalent molecules were potent binders of EZH2 but not EED, SUZ12, or RbAp48. The EZH2-PROTACs might induce the degradation of EZH2 by direct engagement and subsequently initiate the E3 ligase-mediated proteasomal degradation pathway while inducing degradation

of other PRC2 subunits by the EZH2-mediated indirect interaction.

To further investigate the degradation efficiency of E7, we evaluated the levels of PRC2 subunits and H3K27me3 in WSU-DLCL-2 cells exposed to graded concentrations of E7 (0, 0.01, 0.05, 0.1, 0.5, 1.0, 2.5, 5.0, and 10.0 μM) for 48 h. E7 slightly downregulated PRC2 subunit levels at low concen-

Scheme 3. Syntheses of Compounds E7-NC-1 and E7-NC-2^a

^aReagents and conditions: (a) NaH, CH₃I, DMF, 56%; (b) TFA, DCM, 1 h; (c) Ac₂O, 4-hydroxyisobenzofuran-1,3-dione, 140 °C, 6 h, 39% (b, c, two-step yield); (d) 1,1-dibromoheptane, DIPEA, DMF, 85 °C, 3 h, 42%; (e) NaHCO₃, 95 °C, 6 h, 29%; (f) K₂CO₃, CH₃I, DMF, 86%; (g) TFA, DCM, 25 °C, 1 h, Na₂CO₃ neutralization; (h) NaHCO₃, DMF, 95 °C, 3–8 h, 35% (g, h, two-step yield).

trations, but at concentrations over 1 μ M, all PRC2 subunits and H3K27me3 levels were significantly decreased in a dose-dependent manner. Moreover, the PRC2 subunits and H3K27me3 levels rebounded at 10 μ M (Figure 5A), which is consistent with a unique phenomenon of the PROTAC's so-called "hook" effect related to a ternary-complex-mediated mechanism.⁴⁹ Then, we evaluated the levels of PRC2 subunits and H3K27me3 levels in WSU-DLCL-2 cells upon treatment with 1 μ M E7 for various times (0, 0.25, 0.5, 1, 2, 4, 12, 24, 48, 72, and 96 h) by western blot analysis. As shown in Figure 5B, at the early time points (0–2 h), E7 only caused a slight downregulation of the EZH2 protein level but had no obvious effect on other PRC2 subunits. One possible explanation was that E7 may induce rapid degradation of the free EZH2 protein at the beginning of treatment, while a longer time was needed to form the ternary complex to induce the degradation of the PRC2 complex by E7, and the change in H3K27me3 also indirectly confirmed this speculation. All PRC2 subunits and H3K27me3 levels were significantly decreased after 48 h and were completely abolished after 72 h. These results showed that E7 had a powerful and lasting degradation efficiency against PRC2 subunits and the ability to inhibit PRC2 activity.

To investigate the specificity of E7 for PRC2 inhibition, we examined other histone H3 methylation modifications. E7 dose-dependently decreased H3K27me2 and H3K27me3 levels, which rebounded at 10 μ M in WSU-DLCL-2 cells. However, other histone H3 methylation modifications including H3K27me1, H3K9me3, and H3K4me3 were not

affected across all tested concentrations, highlighting the specificity of E7 for PRC2 inhibition (Figure 5C). To exclude the possibility that the downregulation of PRC2 subunits by E7 is cell-specific, we next tested the degradation abilities of E7 in other cancer cell lines. WSU-DLCL-2, SU-DLCL-6, LNCaP, DU 145, A2780, and SKOV3 cancer cell lines were exposed to E7 (1 μ M for 48 h). As illustrated in Figure 5D, E7 significantly decreased PRC2 subunits and H3K27me3 levels in all of the tested cancer cell lines.

Quantitative real-time polymerase chain reaction (PCR) showed that E7 had little effect on the mRNA levels of PRC2 complex subunits including EZH2, SUZ12, EED, and RbAp48 in WSU-DLCL-2 cells (Figure 6A), indicating that E7 induced downregulation of PRC2 subunits without affecting the transcription of PRC2 complex subunits. To further demonstrate that EZH2-targeted PROTACs induced the degradation of the PRC2 complex via the ubiquitin-proteasomal degradation pathway induced by CRBN E3 ligase recruitment, we treated WSU-DLCL-2 cells with E7 in the presence of the CRBN ligand lenalidomide that can compete with PROTAC-mediated binding to the E3 ubiquitin ligase. Lenalidomide treatment alone did not affect the levels of PRC2 complex subunits, but pretreatment with lenalidomide before addition of E7 effectively blocked E7-induced PRC2 subunit degradation. Moreover, proteasome inhibitor MG-132 or the Nedd8-activating enzyme E1 (NAE) inhibitor MLN4924 alone had no effect on PRC2 subunits, while MG-132 or MLN4924 pretreatment before addition of E7 recovered the downregulation of PRC2 subunits (Figure 6B). Furthermore, the

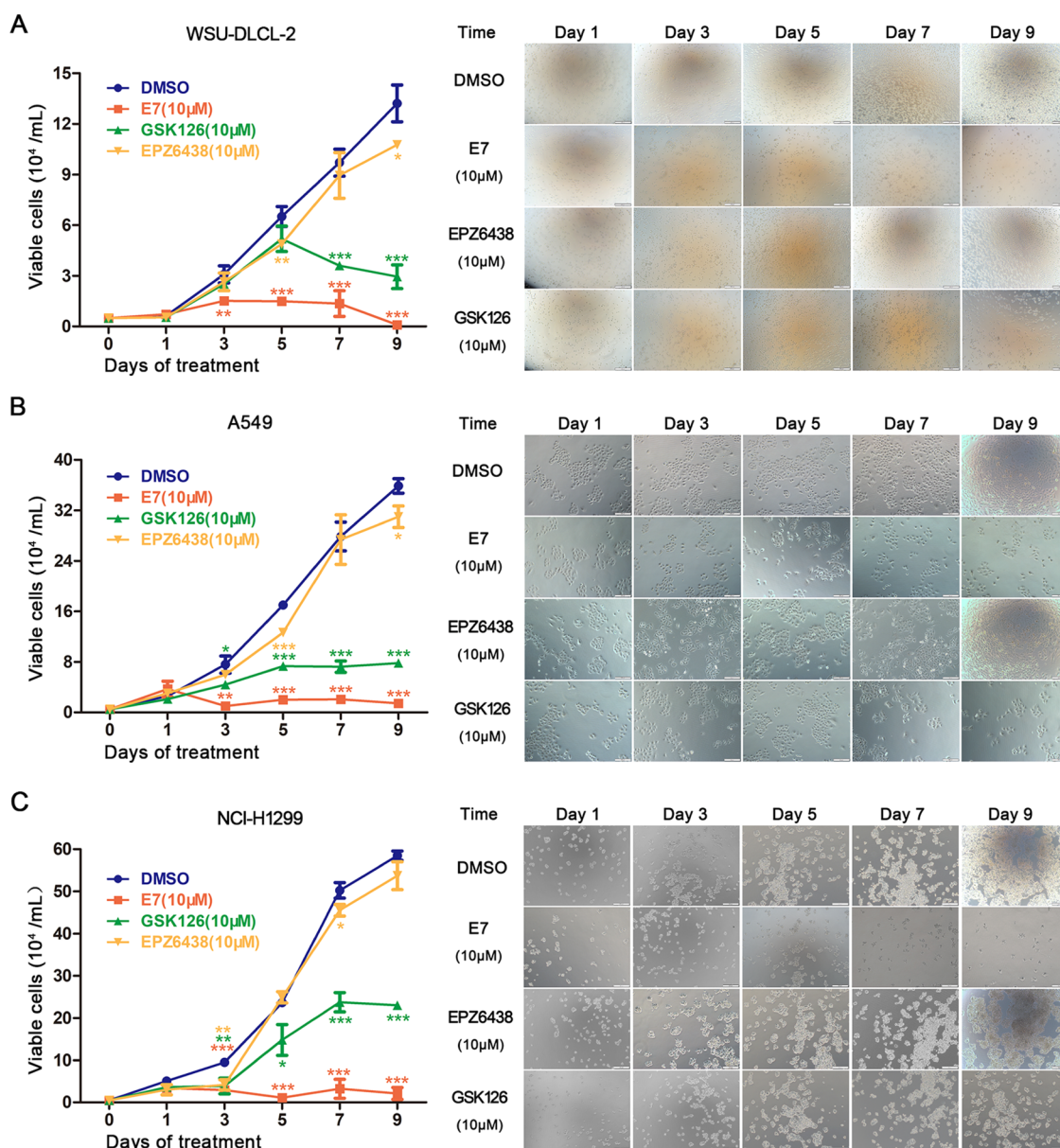


Figure 10. Proliferation curves and optical microscopy images of WSU-DLCL-2 (A), A549 (B), and NCI-H1299 (C) cells treated with E7, EPZ6438, or GSK126 at 10 μ M. Data are expressed as mean \pm SD of three independent experiments, * p < 0.05, ** p < 0.01, and *** p < 0.001, compared with the DMSO-treated group by the t -test.

EED226 had no effect (Figure 6C). These results suggest that the PRC2 subunit depletion induced by E7 resulted from its direct interaction with EZH2 rather than other PRC2 subunits.

We further tested the specificity of E7 by synthesizing E7-NC-1, which resembles E7 but could not bind to CRBN due to a methyl group at the glutarimide ring of thalidomide, and E7-NC-2 with decreased affinity for EZH2 due to an *N*-methyl residue at the pyridone moieties of E7. Synthetic routes of E7-NC-1 and E7-NC-2 are shown in Scheme 3. Briefly, E7-NC-1 was synthesized from 3b, the methylation product of 3-Boc-amino-2,6-dioxopiperidine (3a), according to a similar synthetic route for the preparation of E7. Methylation of 3e with iodomethane and potassium carbonate in DMF afforded 3f, which underwent deprotection of the Boc group and subsequent nucleophilic substitution reaction with 1h to obtain E7-NC-2.

The EZH2 inhibitory potencies of E7, E7-NC-1, and E7-NC-2 were tested by the Alpha-Screen assay. E7-NC-1 demonstrated comparable inhibitory activity against EZH2 to that of E7 (Figure 7A, IC_{50} = 1.9 nM), but E7-NC-2 showed about 10-fold decreased activity against EZH2 compared with E7 (Figure 7B). As expected, the EZH2 inhibitor EPZ6438 and thalidomide did not decrease the PRC2 subunit levels, nor did E7-NC-1 and E7-NC-2 in WSU-DLCL-2 cells (Figure 7C).

To verify the ubiquitination status of all PRC2 complex subunits upon E7 treatment, immunoprecipitation (IP) experiments were carried out with lysates prepared from WSU-DLCL-2 cells treated with E7 at 1 μ M for 48 h. As shown in Figure 8, E7 increased the ubiquitination of EZH2, SUZ12, and EED in WSU-DLCL-2 cells, suggesting that degradation of PRC2 subunits by E7 occurs via the ubiquitin proteasome pathway. Overall, these data indicated that the

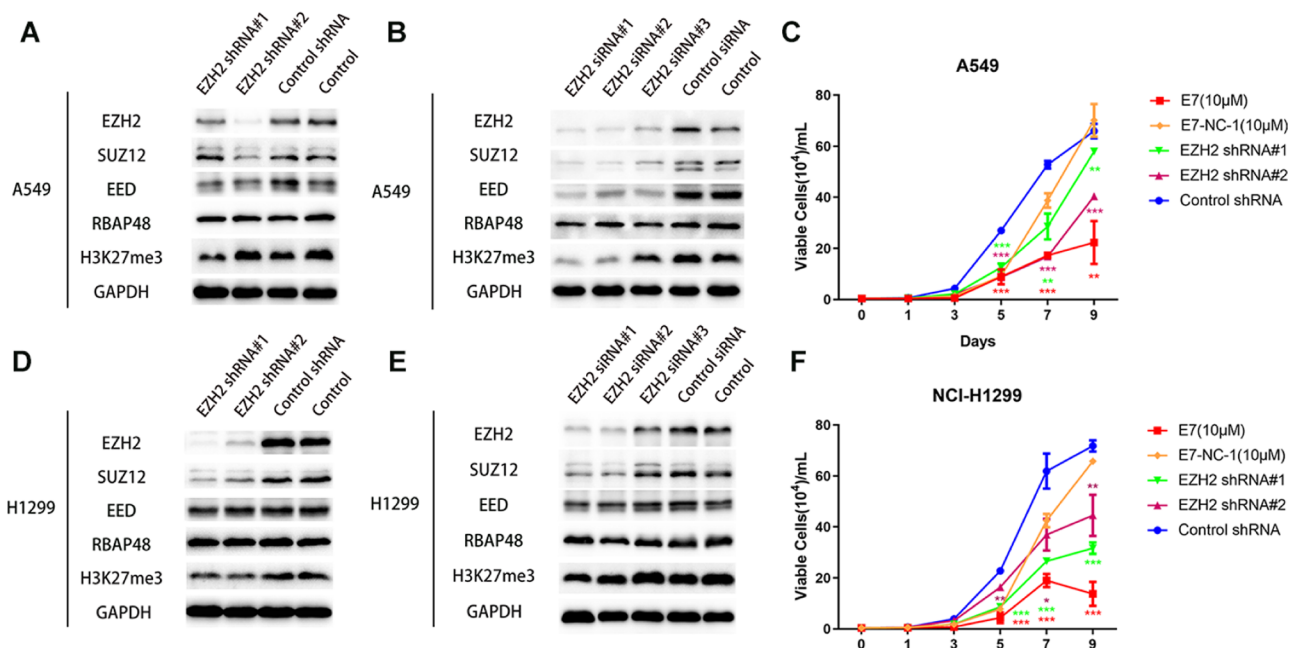


Figure 11. Immunoblot analysis of PRC2 subunits and H3K27me3 expression in A549 (A, B) and H1299 cells (D, E) after treatment with control or EZH2-targeting shRNA. The proliferation curves are for A549 (C) and NCI-H1299 (F) cells after treatment with E7 or E7-NC-1 at 10 μM compared with cells after inducing control or EZH2-targeting shRNA. Data are expressed as mean \pm SD of three independent experiments, * p < 0.05, ** p < 0.01, and *** p < 0.001, compared with the control shRNA group by the t -test.

decrease of PRC2 subunit levels induced by E7 is mediated by the E3-ligase proteasomal degradation pathway.

Several reported H3K27me3-related genes including *ADRB2*, *CDKN2A*, *TXINP*, and *TNFRSF21*, mediated silencing by EZH2/PRC2, were selected for quantitative mRNA expression analysis.^{22,52} In lymphoma cell lines WSU-DLCL-2 and Pfeiffer, the upregulation of *ADRB2* and *TNFRSF21* by E7 treatment was stronger than that of EPZ6438 and GSK126, respectively, while the upregulation of *CDKN2A* and *TXINP* was not as good as that of EPZ6438 and GSK126. In addition, in the lung cancer cell line A549, only *CDKN2A* and *TXINP* were significantly upregulated after E7 treatment (Figure 9A). With a similar extent as those induced by EPZ6438 and GSK126, E7 strongly upregulated the expression of these genes to various extents in different cancer cell lines (Figure 9A).

EZH2 also mediates gene activation including *BRIC5*, *ARL6IP*, *CEP76*, *CENPK*, *CHEK1*, and *TACC3* genes in many cancers, such as lung cancer and breast cancer, which is independent of the catalytic function of EZH2/PRC2.^{6,52} We next analyzed the mRNA levels of these genes in A549, NCI-H1299, and MDA-MB-468 cells after treatment with E7. All of these examined genes were downregulated after treatment with E7 at indicated concentrations (Figure 9B). However, treatment with EPZ6438 or GSK126 did not affect the mRNA expression of these genes (Figure 9B). These data suggested that EZH2 enzymatic inhibitors such as EPZ6438 or GSK126 did not fully block the oncogenic activity of EZH2, whereas EZH2-targeted PROTACs such as E7 completely abolished the oncogenic function of EZH2 implied by the inhibition of the EZH2 noncatalytic function.

The abovementioned results demonstrated that E7 affected both the catalytic and noncatalytic roles of EZH2. Hence, we compared the antiproliferative effects of E7 as well as EZH2 inhibitors EPZ6438 and GSK126 on various cancer cell lines.

DLBCL cells WSU-DLCL-2 (which harbors EZH2-Y641F) and Pfeiffer (which harbors EZH2-A677G) were used to evaluate the antiproliferative effects of E7. Treatment of WSU-DLCL-2 cells with E7 for 3, 5, and 7 days decreased the IC_{50} value from 4.92 to 3.69 μM (Figure S2-A). Better results were obtained for Pfeiffer cells; treatment with E7 for 3, 5, and 7 days decreased the IC_{50} values from 0.49 to 0.21 μM (Figure S2-D). Then, WSU-DLCL-2 cells were chosen to evaluate proliferation for 9 days treated with E7, GSK126, or EPZ6438 alone. EPZ6438 and GSK126 showed potent antiproliferative effects against WSU-DLCL-2 cells (Figure 10A). Remarkably, E7 almost completely inhibited the growth of WSU-DLCL-2 cells, demonstrating the superior antiproliferative effect of EZH2-PROTAC E7 over the other EZH2 inhibitors (Figure 10A).

Since SWI/SNF-mutant cancers depend on the enzymatic and nonenzymatic activities of EZH2 and displayed discrepant responses to EZH2 enzymatic inhibitors, we selected the A549 cell line (SWI/SNF-mutant), which is sensitive to EZH2 inhibitors, and the NCI-H1299 cell line (SWI/SNF-mutant), which is relatively resistant to EZH2 inhibitors, and conducted proliferation assays for 9 days. EPZ6438 had little effect on the proliferation of A549 and NCI-H1299 cells. GSK126 showed a certain degree of antiproliferative activity against A549, with less potency against NCI-H1299 cells (Figure 10B,C), which was consistent with previous reports.³³ E7 demonstrated significant antiproliferative effects against both A549 and NCI-H1299 cell lines (Figures 10B,C and S2-B,C). These results suggested that EZH2-targeted PROTAC E7 showed significant antiproliferative activities against cancer cells dependent on the catalytic and noncatalytic functions of EZH2.

Previous studies showed that knockdown of *EED* can lead to concomitant downregulation of EZH2 and SUZ12.^{50,51} Thus, EED-targeted PROTACs reported by Hsu et al.⁴⁰ and Potjewyd et al.,⁴¹ which induced the downregulation of

EZH2 and SUZ12, may be ascribed to the decreased stability of the PRC2 complex induced by EED degradation. It has also been shown in the literature that genetic knockdown of *EZH2* caused the depletion of SUZ12 and EED besides EZH2 due to the loss of integrity of the PRC2 complex.⁵¹ To verify whether the degradation of PRC2 subunits by E7 results from the loss of integrity of the PRC2 complex, we knocked down *EZH2* by small hairpin RNA (shRNA) in A549 and NCI-H1299 cells. We found that *EZH2* was downregulated in all examined cell lines, and the downregulation of SUZ12 depended on the degree of *EZH2* knockdown. However, the change in the EED level by *EZH2*-shRNA was cell-line-dependent. In addition, the effect of *EZH2*-shRNA on RbAp48 was not as significant as that of EZH2, EED, and SUZ12. Similar results were also observed in A549 and NCI-H1299 cells in which *EZH2* was knocked down by small interfering RNA (siRNA) (Figure 11A,B,D,E). Thus, the mechanism of E7-mediated downregulation of PRC2 subunits may be partially different from that for the genetic knockdown of *EZH2*. We speculated that E7 primarily degrades EZH2 and EED, and the downregulation of EED by E7 might be partially via its recruitment of CRBN to approach EED to initiate subsequent ubiquitin-proteasomal degradation, while the decreased level of SUZ12 may be an indirect outcome of the instability of the PRC2 complex induced by E7.

To verify that the antiproliferative activities of E7 are caused by the degradation of the PRC2 complex, antiproliferative activities of E7 and E7-NC-1 and genetic knockdown of *EZH2* in A549 and H1299 cell lines were evaluated. As shown in Figure 11C,F, E7 exhibited the strongest antiproliferative activity in A549 and NCI-H1299 cell lines, and *EZH2*-shRNA#1 and *EZH2*-shRNA#2 also showed moderate to good antiproliferative activity in both cell lines, while the negative control E7-NC-1 (*EZH2* IC₅₀ = 1.73 nM, Figure 7B) was almost completely inactive. These results indicate that the proliferation inhibitory activity exhibited by PROTAC E7 is related to the degradation of PRC2 subunits.

CONCLUSIONS

Here, we describe the design and synthesis of a potent *EZH2*-targeted PROTAC molecule E7, which induced proteasomal degradation of PRC2 subunits, including EZH2, EED, SUZ12, and RbAp48. Given that *EZH2* mediates both gene silencing via recruitment of the PRC2 complex to catalyze H3K27me3 and PRC2-independent transcriptional activation in various cancers, current *EZH2* inhibitors cannot completely abolish the oncogenic function of *EZH2*. E7 fully suppressed the oncogenic activity of *EZH2* and showed significantly antiproliferative activities of cancers dependent on the catalytic and noncatalytic activities of *EZH2*. In addition, our data suggest that E7 recruits the E3 ubiquitin ligase to the vicinity of the PRC2 complex and results in the indiscriminate ubiquitination and degradation of all PRC2 subunits. It is worth noting that more direct evidence is needed to interpret the mechanism underlying how E7 induces the degradation of proteins such as SUZ12, EED, and RbAp48. Overall, our results shed light on the fact that pharmacological degradation of *EZH2* may offer a potential therapeutic strategy for fully blocking the oncogenic activity of *EZH2*. In general, E7 would be a valuable chemical probe to investigate the biological functions of *EZH2*, and it could also be a promising starting point to develop more potent anticancer drugs for targeting the *EZH2* or PRC2 complex.

EXPERIMENTAL SECTION

Chemistry. All reactions were carried out with magnetic stirring and in dried glassware. Unless otherwise indicated, all chemicals and solvents were purchased from commercial sources and used without purification treatment. Analytical thin-layer chromatography was carried out on 0.20 mm silica gel plates (Haiyang, Qingdao, Shandong, CN) with the QF-254 UV indicator. Column chromatography was conducted using Haiyang silica gel 60 (300–400 mesh). High-resolution mass spectra (HRMS) of all target compounds were performed by a Waters Q-TOF Premier spectrometer with acetonitrile and water as solvents. Nuclear magnetic resonance (NMR) spectra for proton (¹H NMR) and 101 MHz for carbon (¹³C NMR) were acquired on Bruker AVANCE III 400 spectrometers (400 MHz). Peak multiplicity of NMR signals was as follows: s, singlet; d, doublet; t, triplet; q, quartet; m, multiplet. Chemical shift (δ): ppm relative to Me₄Si (internal standard). Coupling constant: J (Hz). High-performance liquid chromatography (HPLC) analysis was performed on the Dionex 1996–2006 Version 6.80 (Phenomenex C18 reversed-column, 4.6 mm \times 150 mm, 5 μ m; gradient elution of methanol/H₂O = 35/65; flow rate, 1.0 mL/min; detection wavelength, 254 nm; temperature, 30 $^{\circ}$ C), and all of the title compounds were of >95% purity.

2-(2,6-Dioxopiperidin-3-yl)-4-hydroxy-2,3-dihydro-1H-isoindole-1,3-dione (1b). A solution of **1a** (3.28 g, 20 mmol, 1.0 equiv) and 3-aminopiperidine-2,6-dione (3.1 g, 24 mmol, 1.2 equiv) in acetic anhydride (50 mL) was stirred at 140 $^{\circ}$ C for 6 h. Then, acetic anhydride was evaporated under reduced pressure, and the residue was poured into water (50 mL). The resulting precipitate was collected by filtration and washed with water to yield **1b** (3.84 g, 71%). HRMS *m/z* calculated for C₁₃H₁₀N₂O₅ [M + H]⁺: 275.0662, found: 275.0686.

General Method to Synthesize 1c–k. A solution of **1b** (1 mmol, 1.0 equiv), DIPEA (3 mmol, 3.0 equiv), and linkers (1.2 mmol, 1.2 equiv) in DMF (10 mL) was stirred at 85–100 $^{\circ}$ C for 3–6 h. The reaction mixture was poured into water and then extracted with ethyl acetate. The organic layer was washed with a saturated solution of NaHCO₃ and brine, dried over Na₂SO₄, concentrated, and purified by column chromatography to afford the corresponding products.

4-[(4-Bromobutoxy)]-2-(2,6-dioxopiperidin-3-yl)-2,3-dihydro-1H-isoindole-1,3-dione (1c). White solid (195.8 mg, 48% yield). ¹H NMR (400 MHz, DMSO-*d*₆) δ 11.08 (s, 1H), 7.82 (m, *J* = 8.5, 7.2 Hz, 1H), 7.52 (d, *J* = 8.5 Hz, 1H), 7.45 (d, *J* = 7.2 Hz, 1H), 5.08 (m, *J* = 12.8, 5.4 Hz, 1H), 4.26 (t, *J* = 6.1 Hz, 2H), 3.66 (t, *J* = 6.7 Hz, 2H), 2.88 (m, *J* = 17.1, 13.9, 5.4 Hz, 1H), 2.57 (m, *J* = 16.4, 12.1 Hz, 2H), 2.03 (m, *J* = 12.5, 8.5, 5.8 Hz, 3H), 1.90 (m, *J* = 8.8, 6.1 Hz, 2H). HRMS *m/z* calculated for C₁₇H₁₇BrN₂O₅ [M + Na]⁺: 431.0213, found: 431.0219.

4-[(5-Bromopentyl)oxy]-2-(2,6-dioxopiperidin-3-yl)-2,3-dihydro-1H-isoindole-1,3-dione (1d). White solid (236.3 mg, 56% yield). ¹H NMR (400 MHz, DMSO-*d*₆) δ 11.08 (s, 1H), 7.81 (m, *J* = 8.5, 7.2 Hz, 1H), 7.52 (d, *J* = 8.5 Hz, 1H), 7.44 (d, *J* = 7.2 Hz, 1H), 5.08 (m, *J* = 12.8, 5.4 Hz, 1H), 4.22 (t, *J* = 6.3 Hz, 2H), 3.56 (t, *J* = 6.7 Hz, 2H), 2.94–2.82 (m, 1H), 2.67–2.53 (m, 2H), 2.03 (m, *J* = 13.5, 6.0, 3.4, 2.9 Hz, 1H), 1.90 (m, *J* = 6.8 Hz, 2H), 1.80 (m, *J* = 6.7 Hz, 2H), 1.59 (m, *J* = 9.6, 6.2 Hz, 2H). HRMS *m/z* calculated for C₁₈H₁₉BrN₂O₅ [M + Na]⁺: 445.0370, found: 445.0367.

4-[(6-Bromohexyl)oxy]-2-(2,6-dioxopiperidin-3-yl)isoindoline-1,3-dione (1e). White solid (161.3 mg, 37% yield). ¹H NMR (400 MHz, DMSO-*d*₆) δ 11.09 (s, 1H), 7.81 (m, *J* = 8.5, 7.3 Hz, 1H), 7.51 (d, *J* = 8.5 Hz, 1H), 7.44 (d, *J* = 7.2 Hz, 1H), 5.08 (m, *J* = 12.8, 5.4 Hz, 1H), 4.21 (t, *J* = 6.3 Hz, 2H), 3.54 (t, *J* = 6.7 Hz, 2H), 2.96–2.82 (m, 1H), 2.67–2.53 (m, 2H), 2.03 (m, *J* = 13.5, 6.5, 6.0, 3.4 Hz, 1H), 1.84 (q, *J* = 6.8 Hz, 2H), 1.76 (q, *J* = 6.7 Hz, 2H), 1.47 (m, *J* = 7.8, 4.5, 4.1 Hz, 4H). HRMS *m/z* calculated for C₁₉H₂₁BrN₂O₅ [M + Na]⁺: 459.0526, found: 459.0523.

4-[(7-Bromoheptyl)oxy]-2-(2,6-dioxopiperidin-3-yl)-2,3-dihydro-1H-isoindole-1,3-dione (1f). White solid (284.0 mg, 63% yield). ¹H NMR (400 MHz, DMSO-*d*₆) δ 11.09 (s, 1H), 7.81 (t, *J* = 7.9 Hz, 1H), 7.51 (d, *J* = 8.5 Hz, 1H), 7.44 (d, *J* = 7.2 Hz, 1H), 5.08 (m, *J* = 12.9, 5.4 Hz, 1H), 4.21 (t, *J* = 6.4 Hz, 2H), 3.53 (t, *J* = 6.7 Hz, 2H),

2.89 (m, $J = 19.1, 14.4, 5.4$ Hz, 1H), 2.59 (d, $J = 17.3$ Hz, 2H), 2.11–1.96 (m, 1H), 1.79 (m, $J = 20.7, 6.6$ Hz, 4H), 1.54–1.30 (m, 6H). HRMS m/z calculated for $C_{20}H_{23}BrN_2O_5$ [$M + H$] $^+$: 451.0863, found: 451.0852.

4-[(8-Bromooctyl)oxy]-2-(2,6-dioxopiperidin-3-yl)-2,3-dihydro-1H-isoindole-1,3-dione (1g). White solid (232.4 mg, 50% yield). 1H NMR (400 MHz, DMSO- d_6) δ 11.08 (s, 1H), 7.80 (m, $J = 8.5, 7.2$ Hz, 1H), 7.51 (d, $J = 8.5$ Hz, 1H), 7.44 (d, $J = 7.2$ Hz, 1H), 5.07 (m, $J = 12.9, 5.4$ Hz, 1H), 4.20 (t, $J = 6.4$ Hz, 2H), 3.52 (t, $J = 6.7$ Hz, 2H), 2.94–2.81 (m, 1H), 2.69–2.52 (m, 2H), 2.03 (m, $J = 14.1, 6.7, 3.3, 2.9$ Hz, 1H), 1.77 (m, $J = 12.4, 6.7$ Hz, 4H), 1.52–1.28 (m, 8H). HRMS m/z calculated for $C_{21}H_{25}BrN_2O_5$ [$M + H$] $^+$: 465.1020, found: 465.0994;

4-[(9-Bromononyl)oxy]-2-(2,6-dioxopiperidin-3-yl)-2,3-dihydro-1H-isoindole-1,3-dione (1h). White solid (292.0 mg, 61% yield). 1H NMR (400 MHz, DMSO- d_6) δ 11.09 (s, 1H), 7.81 (m, $J = 8.5, 7.3$ Hz, 1H), 7.51 (d, $J = 8.5$ Hz, 1H), 7.44 (d, $J = 7.2$ Hz, 1H), 5.08 (m, $J = 12.8, 5.4$ Hz, 1H), 4.20 (t, $J = 6.4$ Hz, 2H), 3.52 (m, $J = 6.7, 2.0$ Hz, 2H), 2.89 (m, $J = 16.8, 13.9, 5.3$ Hz, 1H), 2.58 (m, $J = 16.9, 12.4$ Hz, 2H), 2.09–1.99 (m, 1H), 1.84–1.72 (m, 4H), 1.46 (t, $J = 7.6$ Hz, 2H), 1.37 (d, $J = 7.2$ Hz, 4H), 1.33–1.25 (m, 4H). HRMS m/z calculated for $C_{22}H_{27}BrN_2O_5$ [$M + H$] $^+$: 479.1176, found: 479.1164.

4-[(10-Bromodecyl)oxy]-2-(2,6-dioxopiperidin-3-yl)-2,3-dihydro-1H-isoindole-1,3-dione (1i). White solid (201.7 mg, 41% yield). 1H NMR (400 MHz, DMSO- d_6) δ 11.09 (s, 1H), 7.84–7.75 (m, 1H), 7.51 (d, $J = 8.5$ Hz, 1H), 7.44 (d, $J = 7.2$ Hz, 1H), 5.07 (m, $J = 12.8, 5.4$ Hz, 1H), 4.20 (t, $J = 6.4$ Hz, 2H), 3.52 (m, $J = 6.7, 2.2$ Hz, 2H), 2.88 (m, $J = 17.0, 13.9, 5.4$ Hz, 1H), 2.58 (m, $J = 16.3, 12.2$ Hz, 2H), 2.03 (m, $J = 8.0, 4.4$ Hz, 1H), 1.76 (m, $J = 14.1, 11.4, 6.7$ Hz, 4H), 1.45 (q, $J = 7.4$ Hz, 2H), 1.36 (q, $J = 6.3$ Hz, 4H), 1.30 (d, $J = 18.4$ Hz, 6H). HRMS m/z calculated for $C_{23}H_{29}BrN_2O_5$ [$M + Na$] $^+$: 515.1152, found: 515.1147.

4-[(11-Bromoundecyl)oxy]-2-(2,6-dioxopiperidin-3-yl)-2,3-dihydro-1H-isoindole-1,3-dione (1j). White solid (293.5 mg, 58% yield). 1H NMR (400 MHz, DMSO- d_6) δ 11.08 (s, 1H), 7.80 (t, $J = 7.9$ Hz, 1H), 7.51 (d, $J = 8.6$ Hz, 1H), 7.44 (d, $J = 7.3$ Hz, 1H), 5.07 (m, $J = 13.0, 5.4$ Hz, 1H), 4.20 (t, $J = 6.4$ Hz, 2H), 3.51 (t, $J = 6.7$ Hz, 2H), 2.88 (s, 1H), 2.61 (s, 2H), 2.03 (d, $J = 13.5$ Hz, 1H), 1.76 (t, $J = 9.2$ Hz, 4H), 1.45 (t, $J = 7.8$ Hz, 2H), 1.41–1.33 (m, 4H), 1.27 (s, 8H). HRMS m/z calculated for $C_{24}H_{31}BrN_2O_5$ [$M + Na$] $^+$: 529.1308, found: 529.1298.

4-[(12-Bromododecyl)oxy]-2-(2,6-dioxopiperidin-3-yl)-2,3-dihydro-1H-isoindole-1,3-dione (1k). White solid (176.8 mg, 34% yield). 1H NMR (400 MHz, DMSO- d_6) δ 11.09 (s, 1H), 7.81 (t, $J = 7.8$ Hz, 1H), 7.47 (m, $J = 27.8, 7.8$ Hz, 2H), 5.08 (m, $J = 13.0, 5.5$ Hz, 1H), 4.20 (t, $J = 6.5$ Hz, 2H), 3.51 (t, $J = 6.7$ Hz, 2H), 2.98–2.80 (m, 1H), 2.60 (d, $J = 17.2$ Hz, 2H), 2.15–1.96 (m, 1H), 1.77 (q, $J = 8.6, 8.2$ Hz, 4H), 1.53–1.41 (m, 2H), 1.35 (s, 4H), 1.26 (s, 10H). HRMS m/z calculated for $C_{25}H_{33}BrN_2O_5$ [$M + Na$] $^+$: 543.1465, found: 543.1472.

Methyl 3-Amino-5-bromo-2-methylbenzoate (2b). Methyl 3-bromo-5-nitrobenzoate **2a** (5.5 g, 20 mmol, 1.0 equiv) and ammonium chloride (5.6 g, 100 mmol, 5.0 equiv) were dissolved in water/ethanol mixtures (60 mL, H_2O /methanol = 1:3). When the mixtures were heated to 80 °C, iron powder (11.2 g, 200 mmol, 10.0 equiv) was added under stirring for 1 h. The reaction mixture was filtered through diatomite and washed with methanol. Then, the combined filtrate was evaporated to get a residue, which was dissolved in DCM, washed with water, dried, and concentrated to give **2b** without further purification (4.41 g, 92%). 1H NMR (400 MHz, $CDCl_3$) δ 7.31 (d, $J = 2.6$ Hz, 1H), 6.92 (d, $J = 2.6$ Hz, 1H), 3.87 (s, 3H), 3.82 (s, 2H), 2.26 (s, 3H). HRMS m/z calculated for $C_9H_{10}BrNO_2$ [$M + H$] $^+$: 243.9967, found: 243.9958.

Methyl 5-Bromo-2-methyl-3-[(oxan-4-yl)amino]benzoate (2c). To a solution of **2b** (4 g, 17.4 mmol, 1.0 equiv) and tetrahydro-4-pyridone (4.4 g, 52.2 mmol, 3.0 equiv) in $CDCl_3$ (50 mL), acetic acid (2.1 g, 34.8 mmol, 2.0 equiv) was added dropwise to the reaction mixture and stirred at 30 °C for 3 h. Then, $NaBH(OAc)_3$ (2.7 g, 43.6 mmol, 2.5 equiv) was added slowly and stirred overnight at room temperature. The reaction solvent was evaporated and the residue was

purified by column chromatography, affording the title compound (3.3 g, 57.8%). 1H NMR (400 MHz, $CDCl_3$) δ 7.23 (d, $J = 2.0$ Hz, 1H), 6.84 (d, $J = 2.0$ Hz, 1H), 4.01 (m, $J = 11.9, 3.6$ Hz, 2H), 3.87 (s, 3H), 3.66 (d, $J = 7.4$ Hz, 1H), 3.54 (m, $J = 11.6, 2.3$ Hz, 2H), 3.48 (m, 1H), 2.23 (s, 3H), 2.10–1.99 (m, 2H), 1.51 (m, $J = 13.3, 10.6, 4.3$ Hz, 2H). HRMS m/z calculated for $C_{14}H_{18}BrNO_3$ [$M + H$] $^+$: 328.0542, found: 328.0547.

5-Bromo-3-[ethyl(oxan-4-yl)amino]-2-methylbenzoic Acid (2d). To a solution of **2c** (3 g, 9.1 mmol, 1.0 equiv) and anhydrous acetaldehyde (2.3 g, 27.3 mmol, 3.0 equiv) in 1,2-dichloroethane (25 mL), acetic acid (1.1 g, 18.2 mmol, 2.0 equiv) was added and reacted at 30 °C for 1 h. Then, $NaBH(OAc)_3$ (1.48 g, 23 mmol, 2.5 equiv) was added and stirred overnight at room temperature. The reaction mixture was concentrated under reduced pressure to obtain the crude material, which was purified by column chromatography to afford **2d** (2.3 g, 71.0%). 1H NMR (400 MHz, $CDCl_3$) δ 7.71 (d, $J = 2.0$ Hz, 1H), 7.37 (d, $J = 2.0$ Hz, 1H), 3.96 (d, $J = 12.1$ Hz, 2H), 3.89 (s, 3H), 3.32 (m, $J = 11.3, 2.9$ Hz, 2H), 3.05 (q, $J = 7.1$ Hz, 2H), 2.99–2.85 (m, 1H), 2.45 (s, 3H), 1.80–1.54 (m, 4H), 0.87 (t, $J = 7.0$ Hz, 3H). HRMS m/z calculated for $C_{16}H_{23}BrNO_3$ [$M + H$] $^+$: 356.0861, found: 356.0854.

5-Bromo-3-[ethyl(oxan-4-yl)amino]-2-methylbenzoic Acid (2e). A solution of **2d** (2 g, 5.6 mmol) in 20 mL of MeOH containing 50% aqueous NaOH solution (2 M) was stirred at room temperature overnight and then neutralized by HCl (2 M). The resulting white precipitate was collected by filtration and washed with water to yield **2e** (1.75 g, 91.2%). 1H NMR (400 MHz, DMSO- d_6) δ 13.15 (s, 1H), 7.62 (d, $J = 2.1$ Hz, 1H), 7.49 (d, $J = 2.1$ Hz, 1H), 3.83 (m, $J = 9.5, 2.3$ Hz, 2H), 3.26 (m, $J = 11.6, 2.1$ Hz, 2H), 3.04 (q, $J = 7.1$ Hz, 2H), 3.01–2.92 (m, 1H), 2.40 (s, 3H), 1.66–1.58 (m, 2H), 1.50 (m, $J = 11.7, 4.3$ Hz, 2H), 0.80 (t, $J = 7.0$ Hz, 3H). HRMS m/z calculated for $C_{15}H_{20}BrNO_3$ [$M + H$] $^+$: 342.0699, found: 342.0706.

5-Bromo-N-[(4,6-dimethyl-2-oxo-1,2-dihydropyridin-3-yl)methyl]-3-[ethyl(oxan-4-yl)amino]-2-methylbenzamide (2f). The acid **2e** (1.5 g, 4.4 mmol, 1.1 equiv) and 3-(aminomethyl)-4,6-dimethylpyridin-2(1H)-one (4 mmol, 0.61 g, 1.0 equiv), HOAT (3 mmol, 1.1 g, 0.75 equiv), and EDCI (3 mmol, 1.14 g, 0.75 equiv) were added to DMSO (10 mL). Then, the mixture was reacted at 45 °C for 20 h and then poured into ice-cold water (100 mL). The resulting precipitate was collected and air-dried. The precipitate was purified by column chromatography to afford **2f** (1.42 g, 68%). 1H NMR (400 MHz, DMSO- d_6) δ 11.47 (s, 1H), 8.23 (t, $J = 5.0$ Hz, 1H), 7.31 (d, $J = 2.0$ Hz, 1H), 7.09 (d, $J = 2.0$ Hz, 1H), 5.86 (s, 1H), 4.25 (d, $J = 4.9$ Hz, 2H), 3.83 (m, $J = 10.8, 3.5$ Hz, 2H), 3.28–3.18 (m, 2H), 3.01 (q, $J = 7.0$ Hz, 2H), 2.97–2.89 (m, 1H), 2.54 (s, 1H), 2.19 (s, 3H), 2.15 (s, 3H), 2.11 (s, 3H), 1.60 (d, $J = 12.4$ Hz, 2H), 1.49 (m, $J = 11.7, 4.2$ Hz, 2H). HRMS m/z calculated for $C_{23}H_{30}BrN_3O_3$ [$M + H$] $^+$: 476.1543, found: 476.1552.

N-[(4,6-Dimethyl-2-oxo-1,2-dihydropyridin-3-yl)methyl]-5-[ethyl(oxan-4-yl)amino]-4-methyl-4'-[(piperazin-1-yl)methyl]-[1,1'-biphenyl]-3-carboxamide (2g). To a solution of **2f** (1.2 g, 2.5 mmol, 1.0 equiv), 4-[(4-boc-1-piperazinyl)methyl]phenylboronic acid pinacol ester (1.21 g, 3 mmol, 1.2 equiv) in 1,4-dioxane, and H_2O (4:1, 30 mL) were added K_2CO_3 (3.75 mmol, 0.52 g, 1.5 equiv) and $Pd(dppf)Cl_2$ (0.2 mmol, 146 mg, 8% equiv). The mixture was degassed for 5 min and successively reacted at 100 °C for 8 h. The mixture was diluted with ethyl acetate and filtered through diatomite. Then, the filtrate was evaporated to obtain the residue, which was successively purified by chromatography eluting with DCM/ CH_3OH = 10:1–20:1 to afford the product. To a mixture of coupling products in $CDCl_3$ (25 mL), TFA (1 mL) was added and stirred at 25 °C for 1 h. The mixture was neutralized by the saturated Na_2CO_3 solution (2 M, 5 mL); then, the mixture was extracted and washed with water (25 mL) and brine, dried over Na_2SO_4 , and evaporated, and the residue was purified by column chromatography to give **2g** (1.04 g, 74% yield). 1H NMR (400 MHz, DMSO- d_6) δ 11.47 (s, 1H), 8.63 (s, 1H), 8.20 (t, $J = 5.0$ Hz, 1H), 7.60 (d, $J = 7.9$ Hz, 2H), 7.38 (d, $J = 8.0$ Hz, 3H), 7.28–7.16 (m, 1H), 5.86 (s, 1H), 4.30 (d, $J = 4.9$ Hz, 2H), 3.89–3.77 (m, 2H), 3.57 (s, 2H), 3.25 (t, $J = 11.4$ Hz, 2H), 3.09 (d, $J = 6.2$ Hz, 6H), 3.04–2.98 (m, 1H), 2.57 (t, $J = 4.8$ Hz, 4H), 2.25 (s,

3H), 2.21 (s, 3H), 2.11 (s, 3H), 1.66 (d, $J = 12.3$ Hz, 2H), 1.53 (m, $J = 12.4$, 12.0, 4.1 Hz, 2H), 0.84 (t, $J = 6.9$ Hz, 3H). HRMS m/z calculated for $C_{34}H_{45}N_5O_3$ [$M + H$] $^+$: 572.3595, found: 572.3601.

General Method to Synthesize Target Compounds E4–E12 and G4–G12. To a solution of GSK126 or 2g (0.25 mmol, 1 equiv) and 4-hydroxythalidomide analogues containing the alkyl group 1c–k (0.3 mmol, 1.2 equiv) in DMF (5 mL), $NaHCO_3$ (0.5 mmol, 2.0 equiv) was added and stirred at 85–100 °C for 3–8 h. When the reaction was complete, the residue was extracted with ethyl acetate and water; then, the organic layer was washed successively with water and brine, dried over Na_2SO_4 and evaporated, and the crude mixture was purified by column chromatography to afford the corresponding products.

1-[(2S)-Butan-2-yl]-N-[(4,6-dimethyl-2-oxo-1,2-dihydropyridin-3-yl)methyl]-6-[6-[4-(4-[[2-(2,6-dioxopiperidin-3-yl)-1,3-dioxo-2,3-dihydro-1H-isoindol-4-yl]oxy]butyl)piperazin-1-yl]pyridine-3-yl]-3-methyl-1H-indole-4-carboxamide (G4). White solid (72.1 mg, 34% yield). 1H NMR (400 MHz, $DMSO-d_6$) δ 11.45 (s, 1H), 11.10 (s, 1H), 8.50 (d, $J = 2.6$ Hz, 1H), 8.12 (t, $J = 5.2$ Hz, 1H), 7.91 (m, $J = 8.8$, 2.7 Hz, 1H), 7.81 (t, $J = 7.9$ Hz, 1H), 7.72 (s, 1H), 7.53 (d, $J = 8.5$ Hz, 1H), 7.44 (d, $J = 7.2$ Hz, 1H), 7.25 (s, 1H), 7.17 (s, 1H), 6.89 (d, $J = 8.9$ Hz, 1H), 5.86 (s, 1H), 5.09 (m, $J = 12.9$, 5.4 Hz, 1H), 4.59 (m, $J = 7.0$ Hz, 1H), 4.35 (d, $J = 5.1$ Hz, 2H), 4.26 (t, $J = 6.3$ Hz, 2H), 3.51 (d, $J = 4.9$ Hz, 4H), 2.90 (m, $J = 17.3$, 15.5, 5.3 Hz, 1H), 2.70–2.53 (m, 2H), 2.47 (s, 2H), 2.41 (t, $J = 6.8$ Hz, 2H), 2.24 (s, 3H), 2.16 (s, 3H), 2.11 (s, 3H), 2.08–1.96 (m, 1H), 1.82 (q, $J = 6.9$ Hz, 4H), 1.69 (q, $J = 7.4$ Hz, 2H), 1.40 (d, $J = 6.6$ Hz, 3H), 1.23 (s, 2H), 0.73 (t, $J = 7.3$ Hz, 3H). ^{13}C NMR (101 MHz, $DMSO-d_6$) δ 173.2, 170.4, 169.2, 167.3, 165.8, 160.6, 158.5, 158.5, 156.5, 149.8, 146.0, 143.1, 138.2, 137.5, 136.4, 133.7, 131.2, 130.2, 126.5, 124.9, 123.4, 122.2, 120.3, 116.7, 116.5, 115.6, 110.2, 108.2, 107.2, 107.4, 69.2, 57.8, 53.0, 52.1, 49.2, 45.4, 35.5, 31.4, 30.0, 26.9, 22.9, 22.5, 21.3, 19.4, 18.7, 12.2, 11.2. HRMS m/z calculated for $C_{48}H_{54}N_8O_7$ [$M + H$] $^+$: 855.4188, found: 855.4185.

1-[(2S)-Butan-2-yl]-N-[(4,6-dimethyl-2-oxo-1,2-dihydropyridin-3-yl)methyl]-6-[6-[4-(5-[[2-(2,6-dioxopiperidin-3-yl)-1,3-dioxo-2,3-dihydro-1H-isoindol-4-yl]oxy]pentyl)piperazin-1-yl]pyridine-3-yl]-3-methyl-1H-indole-4-carboxamide (G5). White solid (45.6 mg, 21% yield). 1H NMR (400 MHz, $DMSO-d_6$) δ 11.45 (s, 1H), 11.10 (s, 1H), 8.50 (d, $J = 2.4$ Hz, 1H), 8.12 (t, $J = 5.1$ Hz, 1H), 7.91 (m, $J = 8.8$, 2.6 Hz, 1H), 7.81 (t, $J = 7.9$ Hz, 1H), 7.72 (s, 1H), 7.52 (d, $J = 8.5$ Hz, 1H), 7.44 (d, $J = 7.2$ Hz, 1H), 7.25 (s, 1H), 7.18 (d, $J = 1.4$ Hz, 1H), 6.89 (d, $J = 8.9$ Hz, 1H), 5.86 (s, 1H), 5.08 (m, $J = 12.9$, 5.4 Hz, 1H), 4.59 (m, $J = 6.9$ Hz, 1H), 4.36 (d, $J = 5.1$ Hz, 2H), 4.23 (t, $J = 6.3$ Hz, 2H), 3.51 (t, $J = 4.7$ Hz, 4H), 2.89 (m, $J = 17.3$, 14.0, 5.4 Hz, 1H), 2.66–2.53 (m, 2H), 2.48 (s, 2H), 2.34 (d, $J = 7.4$ Hz, 2H), 2.24 (s, 3H), 2.17 (s, 3H), 2.11 (s, 3H), 2.07–1.99 (m, 1H), 1.80 (m, $J = 8.4$, 4.8 Hz, 4H), 1.53 (m, $J = 19.9$, 7.1 Hz, 4H), 1.41 (d, $J = 6.6$ Hz, 3H), 1.24 (d, $J = 5.1$ Hz, 2H), 0.73 (t, $J = 7.3$ Hz, 3H). ^{13}C NMR (101 MHz, $DMSO-d_6$) δ 173.2, 170.4, 169.2, 167.3, 165.8, 163.6, 158.5, 156.5, 149.8, 146.0, 143.1, 138.2, 137.5, 136.4, 133.7, 131.2, 130.2, 126.5, 124.9, 123.4, 122.2, 120.3, 116.7, 116.5, 115.6, 110.2, 108.2, 107.8, 107.4, 69.3, 58.3, 53.0, 52.0, 49.2, 45.4, 35.5, 31.44, 30.0, 28.8, 26.4, 23.8, 22.5, 21.3, 19.4, 18.7, 12.2, 11.2. HRMS m/z calculated for $C_{49}H_{56}N_8O_7$ [$M + H$] $^+$: 869.4345, found: 869.4343.

1-[(2S)-Butan-2-yl]-N-[(4,6-dimethyl-2-oxo-1,2-dihydropyridin-3-yl)methyl]-6-[6-[4-(6-[[2-(2,6-dioxopiperidin-3-yl)-1,3-dioxo-2,3-dihydro-1H-isoindol-4-yl]oxy]hexyl)piperazin-1-yl]pyridine-3-yl]-3-methyl-1H-indole-4-carboxamide (G6). Light-gray solid (63.3 mg, 29% yield). 1H NMR (400 MHz, $DMSO-d_6$) δ 11.45 (s, 1H), 11.10 (s, 1H), 8.49 (d, $J = 2.5$ Hz, 1H), 8.12 (t, $J = 5.1$ Hz, 1H), 7.90 (m, $J = 8.8$, 2.6 Hz, 1H), 7.81 (t, $J = 7.9$ Hz, 1H), 7.72 (d, $J = 1.5$ Hz, 1H), 7.52 (d, $J = 8.6$ Hz, 1H), 7.44 (d, $J = 7.2$ Hz, 1H), 7.25 (s, 1H), 7.17 (d, $J = 1.4$ Hz, 1H), 6.89 (d, $J = 8.9$ Hz, 1H), 5.86 (s, 1H), 5.08 (m, $J = 12.9$, 5.4 Hz, 1H), 4.60 (m, $J = 6.9$ Hz, 1H), 4.35 (d, $J = 5.1$ Hz, 2H), 4.21 (t, $J = 6.4$ Hz, 2H), 3.50 (t, $J = 4.8$ Hz, 4H), 2.89 (m, $J = 17.5$, 14.1, 5.4 Hz, 1H), 2.66–2.54 (m, 2H), 2.46 (s, 4H), 2.32 (d, $J = 7.2$ Hz, 2H), 2.24 (s, 3H), 2.16 (s, 3H), 2.11 (s, 3H), 2.07–2.00 (m, 1H), 1.86–1.72 (m, 4H), 1.50 (m, $J = 7.5$ Hz, 4H), 1.40 (t, $J = 7.3$ Hz, 3H), 1.23 (s, 2H), 0.73 (t, $J = 7.3$ Hz, 3H). ^{13}C NMR (101 MHz, $DMSO-d_6$) δ 173.2, 170.4, 169.2, 167.3, 165.8, 163.6, 158.5, 156.5,

149.8, 146.0, 143.1, 138.2, 137.5, 136.4, 133.7, 131.2, 130.2, 126.5, 124.9, 123.4, 122.2, 120.3, 116.7, 116.5, 115.6, 110.2, 108.1, 107.8, 107.4, 69.3, 58.3, 53.1, 52.1, 49.2, 45.4, 35.5, 31.4, 30.0, 28.9, 27.0, 26.7, 25.7, 22.5, 21.3, 19.4, 18.7, 12.2, 11.2. HRMS m/z calculated for $C_{50}H_{58}N_8O_7$ [$M + H$] $^+$: 883.4501, found: 882.4502.

1-[(2S)-Butan-2-yl]-N-[(4,6-dimethyl-2-oxo-1,2-dihydropyridin-3-yl)methyl]-6-[6-[4-(7-[[2-(2,6-dioxopiperidin-3-yl)-1,3-dioxo-2,3-dihydro-1H-isoindol-4-yl]oxy]heptyl)piperazin-1-yl]pyridine-3-yl]-3-methyl-1H-indole-4-carboxamide (G7). Gray solid (73.6 mg, 33% yield). 1H NMR (400 MHz, $DMSO-d_6$) δ 11.45 (s, 1H), 11.09 (s, 1H), 8.49 (d, $J = 2.5$ Hz, 1H), 8.12 (t, $J = 5.1$ Hz, 1H), 7.90 (m, $J = 8.8$, 2.6 Hz, 1H), 7.81 (m, $J = 8.5$, 7.3 Hz, 1H), 7.72 (d, $J = 1.5$ Hz, 1H), 7.52 (d, $J = 8.6$ Hz, 1H), 7.44 (d, $J = 7.2$ Hz, 1H), 7.25 (s, 1H), 7.17 (d, $J = 1.5$ Hz, 1H), 6.89 (d, $J = 8.9$ Hz, 1H), 5.86 (s, 1H), 5.08 (m, $J = 12.9$, 5.4 Hz, 1H), 4.60 (q, $J = 6.9$ Hz, 1H), 4.35 (d, $J = 5.1$ Hz, 2H), 4.21 (t, $J = 6.4$ Hz, 2H), 3.50 (s, 4H), 2.88 (m, $J = 17.3$, 14.0, 5.4 Hz, 1H), 2.69–2.54 (m, 2H), 2.49–2.40 (m, 4H), 2.31 (d, $J = 7.6$ Hz, 2H), 2.24 (s, 3H), 2.16 (s, 3H), 2.11 (s, 3H), 2.03 (m, $J = 11.9$, 6.1, 3.5 Hz, 1H), 1.78 (m, $J = 19.7$, 6.9 Hz, 4H), 1.47 (q, $J = 7.6$ Hz, 4H), 1.40 (d, $J = 6.6$ Hz, 3H), 1.34 (m, $J = 9.1$, 4.3 Hz, 2H), 1.24 (d, $J = 4.8$ Hz, 2H), 0.73 (t, $J = 7.3$ Hz, 3H). ^{13}C NMR (101 MHz, $DMSO-d_6$) δ 173.2, 170.4, 169.2, 167.3, 165.8, 163.6, 158.5, 156.5, 149.8, 146.0, 143.1, 138.2, 137.5, 136.4, 133.7, 131.2, 127.9, 126.5, 123.4, 122.2, 120.3, 116.7, 116.5, 115.6, 110.2, 108.1, 107.8, 107.4, 69.28, 58.4, 53.1, 52.1, 49.2, 45.4, 35.5, 31.4, 30.0, 29.0, 28.9, 27.4, 25.74, 22.5, 21.3, 19.4, 18.7, 12.1, 11.2. HRMS m/z calculated for $C_{51}H_{60}N_8O_7$ [$M + H$] $^+$: 897.4658, found: 897.4656.

1-[(2S)-Butan-2-yl]-N-[(4,6-dimethyl-2-oxo-1,2-dihydropyridin-3-yl)methyl]-6-[6-[4-(8-[[2-(2,6-dioxopiperidin-3-yl)-1,3-dioxo-2,3-dihydro-1H-isoindol-4-yl]oxy]octyl)piperazin-1-yl]pyridine-3-yl]-3-methyl-1H-indole-4-carboxamide (G8). White solid (41.6 mg, 18% yield). 1H NMR (400 MHz, $DMSO-d_6$) δ 11.45 (s, 1H), 11.10 (s, 1H), 8.49 (d, $J = 2.6$ Hz, 1H), 8.13 (t, $J = 5.1$ Hz, 1H), 7.90 (m, $J = 8.8$, 2.6 Hz, 1H), 7.80 (m, $J = 8.5$, 7.2 Hz, 1H), 7.72 (d, $J = 1.5$ Hz, 1H), 7.51 (d, $J = 8.6$ Hz, 1H), 7.44 (d, $J = 7.2$ Hz, 1H), 7.25 (s, 1H), 7.17 (d, $J = 1.4$ Hz, 1H), 6.89 (d, $J = 8.9$ Hz, 1H), 5.86 (s, 1H), 5.08 (m, $J = 12.9$, 5.4 Hz, 1H), 4.60 (q, $J = 6.9$ Hz, 1H), 4.35 (d, $J = 5.0$ Hz, 2H), 4.21 (t, $J = 6.3$ Hz, 2H), 3.50 (t, $J = 5.7$ Hz, 4H), 2.88 (m, $J = 17.3$, 14.1, 5.4 Hz, 1H), 2.58 (m, $J = 20.8$, 6.8 Hz, 2H), 2.45 (s, 4H), 2.31 (d, $J = 7.4$ Hz, 2H), 2.24 (s, 3H), 2.16 (s, 3H), 2.11 (s, 3H), 2.07–1.98 (m, 1H), 1.78 (m, $J = 13.8$, 6.7 Hz, 4H), 1.48 (d, $J = 7.1$ Hz, 4H), 1.40 (d, $J = 6.7$ Hz, 3H), 1.31 (d, $J = 10.9$ Hz, 4H), 1.23 (s, 2H), 0.73 (t, $J = 7.3$ Hz, 3H). ^{13}C NMR (101 MHz, $DMSO-d_6$) δ 173.2, 170.4, 169.2, 167.3, 165.8, 163.6, 158.5, 156.5, 149.8, 146.0, 143.1, 138.2, 137.5, 136.4, 133.7, 131.2, 130.2, 126.5, 124.9, 123.4, 122.2, 120.3, 116.7, 116.5, 115.6, 108.1, 107.8, 107.4, 69.3, 58.5, 53.1, 52.1, 49.2, 45.4, 35.5, 31.4, 30.0, 29.4, 29.1, 28.9, 27.4, 26.7, 25.7, 22.5, 21.3, 19.4, 18.7, 12.1, 11.2. HRMS m/z calculated for $C_{52}H_{62}N_8O_7$ [$M + H$] $^+$: 911.4814, found: 911.4819.

1-[(2S)-Butan-2-yl]-N-[(4,6-dimethyl-2-oxo-1,2-dihydropyridin-3-yl)methyl]-6-[6-[4-(9-[[2-(2,6-dioxopiperidin-3-yl)-1,3-dioxo-2,3-dihydro-1H-isoindol-4-yl]oxy]nonyl)piperazin-1-yl]pyridine-3-yl]-3-methyl-1H-indole-4-carboxamide (G9). White solid (85.6 mg, 37% yield). 1H NMR (400 MHz, $DMSO-d_6$) δ 11.45 (s, 1H), 11.11 (s, 1H), 8.49 (d, $J = 2.5$ Hz, 1H), 8.13 (t, $J = 5.1$ Hz, 1H), 7.90 (m, $J = 8.8$, 2.6 Hz, 1H), 7.80 (t, $J = 7.9$ Hz, 1H), 7.72 (s, 1H), 7.51 (d, $J = 8.5$ Hz, 1H), 7.44 (d, $J = 7.2$ Hz, 1H), 7.25 (s, 1H), 7.22–7.13 (m, 1H), 6.89 (d, $J = 8.9$ Hz, 1H), 5.86 (s, 1H), 5.08 (m, $J = 12.9$, 5.4 Hz, 1H), 4.60 (q, $J = 6.9$ Hz, 1H), 4.35 (d, $J = 5.1$ Hz, 2H), 4.20 (t, $J = 6.3$ Hz, 2H), 3.50 (s, 4H), 2.88 (m, $J = 17.8$, 14.4, 5.3 Hz, 1H), 2.68–2.54 (m, 2H), 2.45 (s, 4H), 2.30 (s, 2H), 2.24 (s, 3H), 2.16 (s, 3H), 2.11 (s, 3H), 2.03 (m, $J = 11.6$, 5.8 Hz, 1H), 1.86–1.69 (m, 4H), 1.45 (d, $J = 7.2$ Hz, 4H), 1.40 (d, $J = 6.6$ Hz, 3H), 1.38–1.27 (m, 6H), 1.23 (s, 2H), 0.73 (t, $J = 7.3$ Hz, 3H). ^{13}C NMR (101 MHz, $DMSO-d_6$) δ 173.2, 170.4, 169.2, 167.3, 165.8, 163.6, 158.5, 156.5, 149.8, 146.0, 143.1, 138.2, 137.5, 136.4, 133.7, 131.2, 130.2, 126.5, 124.9, 123.4, 122.2, 120.3, 116.7, 116.5, 115.6, 110.2, 108.1, 107.8, 107.4, 69.3, 58.5, 56.5, 53.1, 52.1, 49.2, 45.4, 35.5, 31.4, 30.0, 29.4, 29.1, 28.9, 27.4, 26.8, 25.7, 22.5, 21.3, 19.4, 18.7, 12.2, 11.2. HRMS m/z calculated for $C_{53}H_{64}N_8O_7$ [$M + H$] $^+$: 925.4971, found: 925.4975.

1-[(2*S*)-Butan-2-yl]-N-[(4,6-dimethyl-2-oxo-1,2-dihydropyridin-3-yl)methyl]-6-[6-[4-(10-[[2-(2,6-dioxopiperidin-3-yl)-1,3-dioxo-2,3-dihydro-1*H*-isoindol-4-yl]oxy]decyl)piperazin-1-yl]pyridine-3-yl]-3-methyl-1*H*-indole-4-carboxamide (**G10**). Light-yellow solid (54.1 mg, 23% yield). ¹H NMR (400 MHz, DMSO-*d*₆) δ 11.46 (s, 1H), 11.12 (s, 1H), 8.49 (d, *J* = 2.5 Hz, 1H), 8.13 (t, *J* = 5.2 Hz, 1H), 7.90 (m, *J* = 8.8, 2.6 Hz, 1H), 7.84–7.76 (m, 1H), 7.72 (d, *J* = 1.5 Hz, 1H), 7.50 (d, *J* = 8.6 Hz, 1H), 7.43 (d, *J* = 7.2 Hz, 1H), 7.25 (s, 1H), 7.18 (d, *J* = 1.4 Hz, 1H), 6.89 (d, *J* = 8.9 Hz, 1H), 5.86 (s, 1H), 5.08 (m, *J* = 12.8, 5.4 Hz, 1H), 4.59 (m, *J* = 6.8 Hz, 1H), 4.36 (d, *J* = 5.1 Hz, 2H), 4.20 (t, *J* = 6.4 Hz, 2H), 3.50 (t, *J* = 4.9 Hz, 4H), 2.89 (m, *J* = 17.3, 14.0, 5.3 Hz, 1H), 2.65–2.53 (m, 2H), 2.45 (t, *J* = 5.0 Hz, 4H), 2.29 (t, *J* = 7.4 Hz, 2H), 2.24 (s, 3H), 2.17 (s, 3H), 2.11 (s, 3H), 2.03 (m, *J* = 13.3, 6.3, 5.8, 3.2 Hz, 1H), 1.86–1.71 (m, 4H), 1.45 (d, *J* = 7.7 Hz, 4H), 1.40 (d, *J* = 6.7 Hz, 3H), 1.29 (s, 8H), 1.23 (s, 2H), 0.73 (t, *J* = 7.3 Hz, 3H). ¹³C NMR (101 MHz, DMSO-*d*₆) δ 173.3, 170.4, 169.3, 167.4, 165.8, 163.7, 158.5, 156.5, 150.1, 145.9, 143.2, 138.2, 137.5, 136.4, 133.6, 131.0, 130.2, 126.5, 124.9, 123.4, 122.1, 120.2, 116.6, 116.4, 115.6, 110.1, 108.2, 107.5, 69.3, 58.4, 53.0, 52.1, 49.2, 45.3, 35.5, 31.4, 29.9, 29.4, 29.1, 28.8, 27.4, 26.6, 25.7, 22.5, 21.3, 19.4, 18.6, 12.1, 11.2. HRMS *m/z* calculated for C₃₄H₄₆N₈O₇ [M + H]⁺: 939.5127, found: 939.5124.

1-[(2*S*)-Butan-2-yl]-N-[(4,6-dimethyl-2-oxo-1,2-dihydropyridin-3-yl)methyl]-6-[6-[4-(11-[[2-(2,6-dioxopiperidin-3-yl)-1,3-dioxo-2,3-dihydro-1*H*-isoindol-4-yl]oxy]undecyl)piperazin-1-yl]pyridine-3-yl]-3-methyl-1*H*-indole-4-carboxamide (**G11**). Light-yellow solid (97.6 mg, 41% yield). ¹H NMR (400 MHz, DMSO-*d*₆) δ 11.45 (s, 1H), 11.10 (s, 1H), 8.49 (d, *J* = 2.5 Hz, 1H), 8.12 (t, *J* = 5.1 Hz, 1H), 7.90 (m, *J* = 8.8, 2.6 Hz, 1H), 7.80 (t, *J* = 7.9 Hz, 1H), 7.72 (s, 1H), 7.50 (d, *J* = 8.5 Hz, 1H), 7.43 (d, *J* = 7.2 Hz, 1H), 7.25 (s, 1H), 7.20–7.11 (m, 1H), 6.89 (d, *J* = 8.9 Hz, 1H), 5.86 (s, 1H), 5.08 (m, *J* = 12.9, 5.4 Hz, 1H), 4.60 (m, *J* = 6.7 Hz, 1H), 4.35 (d, *J* = 5.1 Hz, 2H), 4.20 (t, *J* = 6.4 Hz, 2H), 3.51 (s, 4H), 2.96–2.83 (m, 1H), 2.58 (m, *J* = 15.9, 11.8 Hz, 2H), 2.47 (s, 4H), 2.31 (d, *J* = 7.8 Hz, 2H), 2.24 (s, 3H), 2.16 (s, 3H), 2.11 (s, 3H), 2.03 (m, *J* = 9.3, 4.6 Hz, 1H), 1.86–1.70 (m, 4H), 1.46 (t, *J* = 7.5 Hz, 4H), 1.40 (d, *J* = 6.7 Hz, 3H), 1.28 (s, 12H), 0.73 (t, *J* = 7.3 Hz, 3H). ¹³C NMR (101 MHz, DMSO-*d*₆) δ 173.2, 170.4, 169.2, 167.3, 165.8, 163.6, 158.5, 156.5, 149.8, 146.0, 143.1, 138.2, 137.5, 136.4, 133.7, 131.2, 130.2, 126.5, 124.9, 123.4, 122.2, 120.3, 116.7, 116.5, 115.6, 110.2, 108.1, 107.8, 107.4, 69.3, 58.4, 53.0, 52.1, 49.2, 45.3, 35.5, 31.4, 30.0, 29.4, 29.1, 28.9, 27.4, 26.7, 25.7, 22.5, 21.3, 19.4, 18.7, 12.1, 11.2. HRMS *m/z* calculated for C₃₅H₄₈N₈O₇ [M + H]⁺: 953.5283, found: 953.5284.

1-[(2*S*)-Butan-2-yl]-N-[(4,6-dimethyl-2-oxo-1,2-dihydropyridin-3-yl)methyl]-6-[6-[4-(12-[[2-(2,6-dioxopiperidin-3-yl)-1,3-dioxo-2,3-dihydro-1*H*-isoindol-4-yl]oxy]dodecyl)piperazin-1-yl]pyridine-3-yl]-3-methyl-1*H*-indole-4-carboxamide (**G12**). Yellow solid (33.8 mg, 14% yield). ¹H NMR (400 MHz, DMSO-*d*₆) δ 11.45 (s, 1H), 11.10 (s, 1H), 8.49 (d, *J* = 2.5 Hz, 1H), 8.12 (t, *J* = 5.1 Hz, 1H), 7.90 (m, *J* = 8.8, 2.6 Hz, 1H), 7.80 (m, *J* = 8.5, 7.3 Hz, 1H), 7.72 (d, *J* = 1.5 Hz, 1H), 7.50 (d, *J* = 8.6 Hz, 1H), 7.43 (d, *J* = 7.3 Hz, 1H), 7.25 (s, 1H), 7.17 (d, *J* = 1.4 Hz, 1H), 6.89 (d, *J* = 8.9 Hz, 1H), 5.86 (s, 1H), 5.08 (m, *J* = 12.9, 5.4 Hz, 1H), 4.59 (q, *J* = 6.9 Hz, 1H), 4.34 (t, *J* = 5.7 Hz, 2H), 4.19 (t, *J* = 6.4 Hz, 2H), 3.50 (t, *J* = 5.0 Hz, 4H), 2.88 (m, *J* = 17.4, 14.1, 5.4 Hz, 1H), 2.69–2.52 (m, 2H), 2.46 (d, *J* = 4.8 Hz, 4H), 2.30 (t, *J* = 7.5 Hz, 2H), 2.24 (s, 3H), 2.16 (s, 3H), 2.11 (s, 3H), 2.03 (m, *J* = 15.1, 7.9, 4.2 Hz, 1H), 1.85–1.70 (m, 4H), 1.51–1.43 (m, 4H), 1.40 (d, *J* = 6.7 Hz, 3H), 1.27 (s, 14H), 0.73 (t, *J* = 7.3 Hz, 3H). ¹³C NMR (101 MHz, DMSO-*d*₆) δ 173.2, 170.4, 169.2, 167.3, 165.8, 163.6, 158.5, 156.5, 149.8, 146.0, 138.2, 137.5, 136.4, 133.7, 131.2, 130.2, 126.5, 123.4, 122.2, 120.3, 116.7, 116.5, 115.6, 110.2, 108.1, 107.8, 107.4, 69.3, 58.6, 53.1, 52.1, 49.2, 45.4, 35.5, 31.4, 30.0, 29.5, 29.5, 29.1, 28.9, 27.4, 26.8, 25.7, 22.5, 21.3, 19.4, 18.7, 12.1, 11.2. HRMS *m/z* calculated for C₃₆H₅₀N₈O₇ [M + H]⁺: 967.5440, found: 967.5438.

N-[(4,6-Dimethyl-2-oxo-1,2-dihydropyridin-3-yl)methyl]-4'-[[4-(4-[[2-(2,6-dioxopiperidin-3-yl)-1,3-dioxo-2,3-dihydro-1*H*-isoindol-4-yl]oxy]butyl)piperazin-1-yl]methyl]-5-[ethyl(oxan-4-yl)amino]-4-methyl-[1,1'-biphenyl]-3-carboxamide (**E4**). Light-yellow solid (36.0 mg, 15% yield). ¹H NMR (400 MHz, CDCl₃) δ 12.00 (s, 1H), 9.66 (s, 1H), 8.35 (d, *J* = 2.5 Hz, 1H), 7.71–7.57 (m, 2H), 7.44 (d, *J* = 7.2

Hz, 1H), 7.27–7.15 (m, 4H), 5.91 (s, 1H), 4.93 (m, *J* = 11.9, 5.4 Hz, 1H), 4.54 (d, *J* = 5.9 Hz, 2H), 4.19 (q, *J* = 6.2 Hz, 2H), 3.94 (m, *J* = 11.6, 3.3 Hz, 2H), 3.65–3.52 (m, 4H), 3.41 (s, 1H), 3.31 (m, *J* = 11.3, 2.9 Hz, 2H), 3.08 (q, *J* = 7.0 Hz, 2H), 3.04–2.95 (m, 1H), 2.88–2.68 (m, 3H), 2.58 (t, *J* = 5.0 Hz, 4H), 2.45 (t, *J* = 7.1 Hz, 2H), 2.39 (s, 3H), 2.33 (s, 3H), 2.14 (s, 3H), 2.13–2.05 (m, 1H), 1.92 (t, *J* = 6.8 Hz, 2H), 1.81–1.50 (m, 9H), 0.88 (t, *J* = 7.0 Hz, 3H). ¹³C NMR (101 MHz, CDCl₃) δ 171.7, 168.7, 167.1, 165.1, 158.7, 156.6, 150.7, 149.6, 145.9, 142.6, 139.3, 136.5, 135.9, 135.6, 133.9, 132.8, 125.6, 123.2, 122.1, 120.1, 118.8, 115.7, 109.9, 106.9, 69.3, 67.3, 58.4, 58.3, 52.8, 49.1, 45.3, 41.6, 36.1, 31.4, 30.5, 28.8, 26.3, 24.0, 22.7, 19.7, 18.7, 14.7, 12.8. HRMS *m/z* calculated for C₅₁H₆₂N₇O₈ [M + H]⁺: 900.4654, found: 900.4653.

N-[(4,6-Dimethyl-2-oxo-1,2-dihydropyridin-3-yl)methyl]-4'-[[4-(5-[[2-(2,6-dioxopiperidin-3-yl)-1,3-dioxo-2,3-dihydro-1*H*-isoindol-4-yl]oxy]pentyl)piperazin-1-yl]methyl]-5-[ethyl(oxan-4-yl)amino]-4-methyl-[1,1'-biphenyl]-3-carboxamide (**E5**). Yellow solid (61.7 mg, 27% yield). ¹H NMR (400 MHz, DMSO-*d*₆) δ 11.45 (s, 1H), 11.08 (s, 1H), 8.17 (t, *J* = 5.0 Hz, 1H), 7.80 (t, *J* = 7.9 Hz, 1H), 7.57 (d, *J* = 7.9 Hz, 2H), 7.51 (d, *J* = 8.5 Hz, 1H), 7.43 (d, *J* = 7.2 Hz, 1H), 7.42–7.38 (m, 1H), 7.35 (d, *J* = 7.8 Hz, 2H), 7.22 (d, *J* = 1.7 Hz, 1H), 5.86 (s, 1H), 5.07 (m, *J* = 12.9, 5.4 Hz, 1H), 4.30 (d, *J* = 5.0 Hz, 2H), 4.23 (t, *J* = 6.3 Hz, 2H), 3.88–3.78 (m, 2H), 3.46 (s, 2H), 3.25 (t, *J* = 11.4 Hz, 2H), 3.09 (q, *J* = 7.2 Hz, 2H), 3.01 (d, *J* = 10.6 Hz, 1H), 2.94–2.82 (m, 1H), 2.57 (m, *J* = 15.3, 11.4 Hz, 2H), 2.45–2.29 (m, 8H), 2.25 (s, 3H), 2.21 (s, 3H), 2.11 (s, 3H), 2.07–1.97 (m, 1H), 1.83–1.71 (m, 2H), 1.71–1.59 (m, 4H), 1.59–1.48 (m, 2H), 1.25 (d, *J* = 13.0 Hz, 4H), 0.84 (t, *J* = 6.9 Hz, 3H). ¹³C NMR (101 MHz, DMSO-*d*₆) δ 173.2, 170.4, 169.5, 167.3, 165.8, 163.5, 156.5, 149.9, 149.3, 143.2, 140.1, 138.9, 137.9, 137.5, 137.5, 133.7, 133.1, 129.9, 126.8, 123.4, 122.1, 121.3, 120.3, 116.7, 115.6, 107.8, 69.2, 66.8, 62.2, 58.3, 57.7, 53.2, 49.2, 41.7, 35.4, 31.4, 30.8, 29.5, 26.8, 22.9, 22.5, 19.4, 18.7, 15.0, 13.2. HRMS *m/z* calculated for C₅₂H₆₄N₇O₈ [M + H]⁺: 914.4811, found: 914.4812.

N-[(4,6-Dimethyl-2-oxo-1,2-dihydropyridin-3-yl)methyl]-4'-[[4-(6-[[2-(2,6-dioxopiperidin-3-yl)-1,3-dioxo-2,3-dihydro-1*H*-isoindol-4-yl]oxy]hexyl)piperazin-1-yl]methyl]-5-[ethyl(oxan-4-yl)amino]-4-methyl-[1,1'-biphenyl]-3-carboxamide (**E6**). Yellow solid (46.4 mg, 20% yield). ¹H NMR (400 MHz, DMSO-*d*₆) δ 11.45 (s, 1H), 11.09 (s, 1H), 8.17 (t, *J* = 5.0 Hz, 1H), 7.80 (t, *J* = 7.9 Hz, 1H), 7.57 (d, *J* = 7.8 Hz, 2H), 7.51 (d, *J* = 8.5 Hz, 1H), 7.44 (d, *J* = 7.2 Hz, 1H), 7.40 (s, 1H), 7.35 (d, *J* = 7.9 Hz, 2H), 7.22 (s, 1H), 5.86 (s, 1H), 5.07 (m, *J* = 12.9, 5.4 Hz, 1H), 4.29 (d, *J* = 5.0 Hz, 2H), 4.20 (t, *J* = 6.4 Hz, 2H), 3.83 (d, *J* = 11.2 Hz, 2H), 3.47 (s, 2H), 3.24 (d, *J* = 11.3 Hz, 2H), 3.06 (m, *J* = 18.9, 11.1 Hz, 3H), 2.88 (q, *J* = 12.5 Hz, 1H), 2.58 (d, *J* = 17.5 Hz, 2H), 2.38 (s, 6H), 2.25 (s, 3H), 2.21 (s, 3H), 2.11 (s, 3H), 2.03–1.99 (m, 1H), 1.75 (m, *J* = 7.0 Hz, 2H), 1.67 (d, *J* = 12.0 Hz, 2H), 1.49 (m, *J* = 24.8, 6.0 Hz, 4H), 1.38–1.31 (m, 2H), 1.24 (d, *J* = 6.6 Hz, 6H), 0.84 (q, *J* = 6.9 Hz, 3H). ¹³C NMR (101 MHz, CDCl₃) δ 173.3, 170.4, 169.7, 167.3, 165.8, 163.5, 156.5, 150.3, 149.4, 143.3, 140.0, 137.6, 133.7, 133.1, 130.0, 126.8, 123.4, 122.0, 121.2, 121.0, 120.3, 116.6, 115.6, 108.1, 69.2, 66.8, 58.3, 52.9, 49.2, 41.7, 35.4, 31.4, 30.8, 30.7, 29.4, 29.1, 28.7, 25.6, 22.5, 19.4, 18.6, 15.0, 13.1. HRMS *m/z* calculated for C₅₃H₆₆N₇O₈ [M + H]⁺: 928.4967, found: 928.4982.

N-[(4,6-Dimethyl-2-oxo-1,2-dihydropyridin-3-yl)methyl]-4'-[[4-(7-[[2-(2,6-dioxopiperidin-3-yl)-1,3-dioxo-2,3-dihydro-1*H*-isoindol-4-yl]oxy]heptyl)piperazin-1-yl]methyl]-5-[ethyl(oxan-4-yl)amino]-4-methyl-[1,1'-biphenyl]-3-carboxamide (**E7**). Yellow solid (101.3 mg, 43% yield). ¹H NMR (400 MHz, DMSO-*d*₆) δ 11.45 (s, 1H), 11.10 (s, 1H), 8.17 (t, *J* = 5.0 Hz, 1H), 7.80 (t, *J* = 7.9 Hz, 1H), 7.56 (d, *J* = 7.8 Hz, 2H), 7.50 (d, *J* = 8.6 Hz, 1H), 7.43 (d, *J* = 7.3 Hz, 1H), 7.40 (s, 1H), 7.35 (d, *J* = 7.8 Hz, 2H), 7.22 (s, 1H), 5.86 (s, 1H), 5.08 (m, *J* = 12.9, 5.4 Hz, 1H), 4.30 (d, *J* = 4.9 Hz, 2H), 4.20 (t, *J* = 6.4 Hz, 2H), 3.83 (d, *J* = 11.1 Hz, 2H), 3.47 (s, 2H), 3.28–3.20 (m, 2H), 3.09 (q, *J* = 7.6, 7.1 Hz, 2H), 3.01 (d, *J* = 10.7 Hz, 1H), 2.89 (m, *J* = 13.6, 12.5, 6.9 Hz, 1H), 2.59 (d, *J* = 17.0 Hz, 2H), 2.37 (s, 6H), 2.25 (s, 3H), 2.21 (s, 3H), 2.11 (s, 3H), 2.03 (d, *J* = 12.5 Hz, 1H), 1.75 (t, *J* = 7.2 Hz, 2H), 1.67 (d, *J* = 12.0 Hz, 2H), 1.53 (m, *J* = 12.5, 7.6 Hz, 2H), 1.43 (m, *J* = 7.4 Hz, 4H), 1.33 (d, *J* = 6.3 Hz, 2H), 1.28 (d, *J* = 7.8 Hz, 2H), 1.23 (s, 4H), 0.83 (t, *J* = 7.0 Hz, 3H). ¹³C NMR (101

MHz, DMSO- d_6) δ 173.3, 170.4, 169.7, 167.3, 165.8, 163.6, 156.5, 150.3, 149.4, 143.3, 140.0, 139.0, 137.6, 137.6, 137.5, 133.7, 133.1, 130.0, 126.8, 123.4, 122.0, 121.2, 120.2, 116.6, 115.6, 108.1, 69.3, 66.8, 62.0, 58.3, 58.1, 53.0, 52.6, 49.2, 41.7, 35.4, 31.4, 30.8, 29.4, 28.9, 28.8, 27.2, 26.2, 25.7, 22.5, 19.4, 18.6, 15.0, 13.1. HRMS m/z calculated for $C_{54}H_{68}N_7O_8$ $[M + H]^+$: 942.5124, found: 942.5135.

N-[[4,6-Dimethyl-2-oxo-1,2-dihydropyridin-3-yl)methyl]-4'-[[4-(8-[[2-(2,6-dioxopiperidin-3-yl)-1,3-dioxo-2,3-dihydro-1H-isoindol-4-yl]oxy]octyl)piperazin-1-yl]methyl]-5-[ethyl(oxan-4-yl)amino]-4-methyl-[1,1'-biphenyl]-3-carboxamide (**E8**). Yellow solid (69.3 mg, 29% yield). 1H NMR (400 MHz, DMSO- d_6) δ 11.45 (s, 1H), 11.09 (s, 1H), 8.17 (t, J = 5.0 Hz, 1H), 7.80 (t, J = 7.9 Hz, 1H), 7.56 (d, J = 7.8 Hz, 2H), 7.50 (d, J = 8.6 Hz, 1H), 7.43 (d, J = 7.2 Hz, 1H), 7.40 (d, J = 2.1 Hz, 1H), 7.35 (d, J = 7.9 Hz, 2H), 7.22 (d, J = 1.9 Hz, 1H), 5.86 (s, 1H), 5.07 (m, J = 12.9, 5.4 Hz, 1H), 4.30 (d, J = 5.0 Hz, 2H), 4.19 (t, J = 6.4 Hz, 2H), 3.88–3.77 (m, 2H), 3.47 (s, 2H), 3.25 (t, J = 11.8 Hz, 2H), 3.09 (q, J = 7.1 Hz, 2H), 3.02 (q, J = 6.9, 5.4 Hz, 1H), 2.88 (m, J = 17.5, 14.2, 5.3 Hz, 1H), 2.63–2.54 (m, 2H), 2.46–2.30 (m, 6H), 2.25 (s, 5H), 2.21 (s, 3H), 2.11 (s, 3H), 2.06–2.00 (m, 1H), 1.75 (t, J = 7.3 Hz, 2H), 1.66 (d, J = 12.0 Hz, 2H), 1.54 (m, J = 11.8, 4.0 Hz, 2H), 1.43 (m, J = 11.6, 6.5 Hz, 4H), 1.36–1.20 (m, 8H), 0.83 (t, J = 6.9 Hz, 3H). ^{13}C NMR (101 MHz, DMSO- d_6) δ 173.2, 170.4, 169.5, 167.3, 165.8, 163.5, 156.5, 150.0, 149.3, 143.2, 140.1, 139.0, 137.5, 133.7, 133.1, 129.9, 126.8, 123.4, 122.1, 121.3, 120.3, 116.7, 115.6, 107.8, 69.3, 66.8, 62.2, 58.3, 53.2, 49.2, 41.7, 35.4, 31.4, 30.8, 29.3, 29.1, 28.9, 27.3, 26.6, 25.7, 22.5, 19.4, 18.7, 15.0, 13.2. HRMS m/z calculated for $C_{55}H_{70}N_7O_8$ $[M + H]^+$: 956.5280, found: 956.5281.

N-[[4,6-Dimethyl-2-oxo-1,2-dihydropyridin-3-yl)methyl]-4'-[[4-(9-[[2-(2,6-dioxopiperidin-3-yl)-1,3-dioxo-2,3-dihydro-1H-isoindol-4-yl]oxy]nonyl)piperazin-1-yl]methyl]-5-[ethyl(oxan-4-yl)amino]-4-methyl-[1,1'-biphenyl]-3-carboxamide (**E9**). Yellow solid (97.1 mg, 40% yield). 1H NMR (400 MHz, DMSO- d_6) δ 11.45 (s, 1H), 11.10 (s, 1H), 8.18 (q, J = 5.6, 5.0 Hz, 1H), 7.80 (t, J = 7.9 Hz, 1H), 7.56 (d, J = 7.8 Hz, 2H), 7.51 (d, J = 8.5 Hz, 1H), 7.43 (d, J = 7.3 Hz, 1H), 7.40 (d, J = 1.9 Hz, 1H), 7.35 (d, J = 7.9 Hz, 2H), 7.22 (d, J = 1.8 Hz, 1H), 5.86 (s, 1H), 5.07 (m, J = 12.9, 5.4 Hz, 1H), 4.29 (d, J = 4.9 Hz, 2H), 4.19 (t, J = 6.4 Hz, 2H), 3.83 (d, J = 11.1 Hz, 2H), 3.47 (s, 2H), 3.24 (d, J = 11.3 Hz, 2H), 3.09 (q, J = 7.1 Hz, 2H), 3.01 (q, J = 7.2, 5.6 Hz, 1H), 2.89 (m, J = 13.4, 12.1, 6.9 Hz, 1H), 2.57 (m, J = 15.9, 12.0 Hz, 2H), 2.37 (s, 6H), 2.25 (s, 5H), 2.21 (s, 3H), 2.11 (s, 3H), 2.05–1.99 (m, 1H), 1.75 (m, J = 6.6 Hz, 2H), 1.66 (d, J = 12.1 Hz, 2H), 1.54 (m, J = 11.9, 4.1 Hz, 2H), 1.45 (t, J = 7.7 Hz, 2H), 1.40 (d, J = 8.9 Hz, 2H), 1.33 (d, J = 5.8 Hz, 2H), 1.25 (d, J = 11.4 Hz, 8H), 0.84 (q, J = 7.0 Hz, 3H). ^{13}C NMR (101 MHz, DMSO- d_6) δ 173.3, 170.4, 169.6, 167.3, 165.8, 163.5, 156.5, 150.2, 149.4, 143.3, 140.0, 139.0, 137.5, 133.7, 133.1, 130.0, 126.8, 123.4, 122.0, 121.2, 120.3, 116.6, 115.6, 108.0, 69.3, 66.8, 62.1, 58.3, 53.0, 52.6, 49.2, 41.7, 35.4, 31.4, 30.8, 29.3, 29.2, 29.0, 28.8, 27.3, 25.7, 22.5, 19.4, 18.6, 15.0, 13.2. HRMS m/z calculated for $C_{56}H_{72}N_7O_8$ $[M + H]^+$: 970.5437, found: 970.5474.

N-[[4,6-Dimethyl-2-oxo-1,2-dihydropyridin-3-yl)methyl]-4'-[[4-(10-[[2-(2,6-dioxopiperidin-3-yl)-1,3-dioxo-2,3-dihydro-1H-isoindol-4-yl]oxy]decyl)piperazin-1-yl]methyl]-5-[ethyl(oxan-4-yl)amino]-4-methyl-[1,1'-biphenyl]-3-carboxamide (**E10**). Light-yellow solid (81.2 mg, 33% yield). 1H NMR (400 MHz, DMSO- d_6) δ 11.44 (s, 1H), 11.10 (s, 1H), 8.17 (t, J = 5.0 Hz, 1H), 7.80 (t, J = 7.9 Hz, 1H), 7.56 (d, J = 7.9 Hz, 2H), 7.50 (d, J = 8.5 Hz, 1H), 7.43 (d, J = 7.3 Hz, 1H), 7.39 (d, J = 1.8 Hz, 1H), 7.35 (d, J = 7.9 Hz, 2H), 7.22 (d, J = 1.8 Hz, 1H), 5.85 (s, 1H), 5.07 (m, J = 12.9, 5.3 Hz, 1H), 4.29 (d, J = 5.0 Hz, 2H), 4.19 (d, J = 6.5 Hz, 2H), 3.86–3.78 (m, 2H), 3.47 (s, 2H), 3.24 (d, J = 11.3 Hz, 2H), 3.09 (q, J = 7.2 Hz, 2H), 3.01 (d, J = 11.0 Hz, 1H), 2.88 (m, J = 18.0, 14.1, 5.3 Hz, 1H), 2.68–2.54 (m, 2H), 2.35 (d, J = 16.6 Hz, 6H), 2.25 (s, 5H), 2.21 (s, 3H), 2.10 (s, 3H), 2.06–1.98 (m, 1H), 1.75 (m, J = 6.6 Hz, 2H), 1.66 (d, J = 11.4 Hz, 2H), 1.53 (m, J = 12.2, 5.9 Hz, 2H), 1.45 (t, J = 7.8 Hz, 2H), 1.42–1.31 (m, 4H), 1.25 (d, J = 8.1 Hz, 10H), 0.83 (t, J = 6.9 Hz, 3H). ^{13}C NMR (101 MHz, DMSO- d_6) δ 173.2, 170.4, 167.3, 166.1, 165.6, 164.0, 161.2, 156.5, 149.9, 149.3, 137.5, 133.1, 129.9, 126.8, 121.3, 120.3, 116.7, 115.6, 106.4, 76.6, 69.3, 67.7, 64.1, 58.4, 53.1, 49.2, 35.4, 34.7, 31.4, 29.4, 29.1, 28.9, 26.3, 25.5, 22.5, 22.2, 19.0,

18.4, 18.0, 16.8, 15.0, 14.6, 11.4. HRMS m/z calculated for $C_{57}H_{74}N_7O_8$ $[M + H]^+$: 984.5593, found: 984.5593.

N-[[4,6-Dimethyl-2-oxo-1,2-dihydropyridin-3-yl)methyl]-4'-[[4-(11-[[2-(2,6-dioxopiperidin-3-yl)-1,3-dioxo-2,3-dihydro-1H-isoindol-4-yl]oxy]undecyl)piperazin-1-yl]methyl]-5-[ethyl(oxan-4-yl)amino]-4-methyl-[1,1'-biphenyl]-3-carboxamide (**E11**). Yellow solid (119.8 mg, 47% yield). 1H NMR (400 MHz, DMSO- d_6) δ 11.44 (s, 1H), 11.09 (s, 1H), 8.17 (t, J = 5.0 Hz, 1H), 7.80 (t, J = 7.9 Hz, 1H), 7.56 (d, J = 7.8 Hz, 2H), 7.51 (d, J = 8.6 Hz, 1H), 7.43 (d, J = 7.3 Hz, 1H), 7.39 (d, J = 1.8 Hz, 1H), 7.35 (d, J = 8.0 Hz, 2H), 7.22 (d, J = 1.8 Hz, 1H), 5.86 (s, 1H), 5.07 (m, J = 12.8, 5.4 Hz, 1H), 4.29 (d, J = 4.9 Hz, 2H), 4.19 (t, J = 6.4 Hz, 2H), 3.83 (d, J = 11.2 Hz, 2H), 3.47 (s, 2H), 3.24 (d, J = 11.3 Hz, 2H), 3.09 (q, J = 7.1 Hz, 2H), 3.01 (d, J = 10.7 Hz, 1H), 2.88 (m, J = 18.6, 14.5, 5.3 Hz, 1H), 2.58 (d, J = 17.4 Hz, 2H), 2.37 (s, 6H), 2.24 (s, 4H), 2.21 (s, 3H), 2.10 (s, 3H), 2.06–1.96 (m, 2H), 1.75 (t, J = 7.3 Hz, 2H), 1.66 (d, J = 12.4 Hz, 2H), 1.52 (m, J = 12.1, 3.9 Hz, 2H), 1.45 (s, 2H), 1.34 (s, 4H), 1.24 (d, J = 4.5 Hz, 12H), 0.83 (t, J = 7.5 Hz, 3H). ^{13}C NMR (101 MHz, CDCl $_3$) δ 171.6, 170.1, 168.7, 167.1, 165.7, 165.2, 158.7, 156.7, 150.7, 149.6, 146.0, 142.6, 139.4, 136.4, 136.1, 135.8, 135.6, 133.9, 132.8, 125.5, 123.2, 122.1, 120.1, 118.9, 117.2, 115.6, 109.9, 106.8, 77.3, 69.5, 67.3, 58.7, 58.4, 52.9, 49.1, 45.2, 41.6, 36.2, 31.5, 30.5, 29.5, 29.4, 29.3, 29.2, 28.9, 27.5, 26.7, 25.7, 22.7, 19.7, 18.7, 14.7, 12.8. HRMS m/z calculated for $C_{58}H_{76}N_7O_8$ $[M + H]^+$: 998.5750, found: 998.5775.

N-[[4,6-Dimethyl-2-oxo-1,2-dihydropyridin-3-yl)methyl]-4'-[[4-(12-[[2-(2,6-dioxopiperidin-3-yl)-1,3-dioxo-2,3-dihydro-1H-isoindol-4-yl]oxy]dodecyl)piperazin-1-yl]methyl]-5-[ethyl(oxan-4-yl)amino]-4-methyl-[1,1'-biphenyl]-3-carboxamide (**E12**). Yellow solid (48.1 mg, 19% yield). 1H NMR (400 MHz, DMSO- d_6) δ 11.44 (s, 1H), 11.09 (s, 1H), 8.17 (t, J = 4.9 Hz, 1H), 7.82–7.75 (m, 1H), 7.60–7.53 (m, 2H), 7.50 (m, J = 8.6, 1.9 Hz, 1H), 7.43 (m, J = 7.3, 1.6 Hz, 1H), 7.39 (d, J = 2.0 Hz, 1H), 7.38–7.31 (m, 2H), 7.22 (d, J = 1.8 Hz, 1H), 5.85 (s, 1H), 5.07 (m, J = 12.9, 5.3 Hz, 1H), 4.29 (d, J = 4.9 Hz, 2H), 4.22–4.14 (m, 2H), 3.83 (d, J = 11.1 Hz, 2H), 3.46 (s, 2H), 3.23 (d, J = 11.3 Hz, 2H), 3.08 (q, J = 7.1 Hz, 2H), 3.00 (d, J = 11.1 Hz, 1H), 2.88 (m, J = 18.9, 14.2, 5.4 Hz, 1H), 2.57 (m, J = 15.5, 11.9 Hz, 2H), 2.37 (s, 6H), 2.24 (s, 5H), 2.21 (s, 3H), 2.10 (s, 3H), 2.06–1.97 (m, 1H), 1.74 (t, J = 7.2 Hz, 2H), 1.66 (d, J = 12.3 Hz, 2H), 1.53 (m, J = 11.9, 4.0 Hz, 2H), 1.49–1.41 (m, 2H), 1.35 (m, J = 16.7, 5.5 Hz, 4H), 1.25 (d, J = 7.7 Hz, 14H), 0.83 (t, J = 6.9 Hz, 3H). ^{13}C NMR (101 MHz, DMSO- d_6) δ 173.2, 170.4, 169.5, 167.3, 165.8, 163.5, 156.5, 149.9, 149.3, 143.2, 140.1, 139.0, 137.5, 133.7, 129.9, 126.8, 122.1, 121.3, 120.3, 116.7, 115.6, 107.8, 69.3, 66.8, 62.2, 58.3, 53.3, 53.1, 49.2, 41.7, 35.4, 31.4, 30.8, 29.5, 29.4, 29.4, 29.1, 28.9, 27.4, 26.7, 25.7, 22.5, 19.4, 18.7, 15.0, 13.2. HRMS m/z calculated for $C_{59}H_{78}N_7O_8$ $[M + H]^+$: 1012.5906, found: 1012.5910.

tert-Butyl (1-Methyl-2,6-dioxopiperidin-3-yl)carbamate (3b). To a solution of **3a** (456 mg, 2 mmol) in DMF (10 mL), NaH (60%, 87.8 mg) was slowly added and stirred for 10 min at 0 °C. CH $_3$ I (0.19 mL, 3 mmol) was added dropwise by a syringe and reacted for 2 h at 25 °C. The reaction residue was extracted with ethyl acetate and aqueous HCl (1 N, 20 mL). The organic layer was washed with water, dried over Na $_2$ SO $_4$, and evaporated under a vacuum. The crude product was purified by column chromatography to afford **3b** as a white solid (272 mg, 56%). 1H NMR (400 MHz, DMSO- d_6) δ 7.19 (d, J = 8.8 Hz, 1H), 4.30 (m, 1H), 2.80 (m, Hz, 1H), 2.64 (m, 1H), 2.02–1.85 (m, 2H), 1.40 (s, 9H). HRMS m/z calculated for $C_{11}H_{19}N_2O_4$ $[M + H]^+$: 243.1339, found: 243.1341.

4-Hydroxy-2-(1-methyl-2,6-dioxopiperidin-3-yl)-2,3-dihydro-1H-isoindole-1,3-dione (3c). To a solution of **3b** (242 mg, 1 mmol) in DCM (10 mL), TFA (1 mL) was added and stirred at 25 °C for 1 h. When the reaction was complete, the crude mixture was evaporated under reduced pressure. Then, residues were used in the next step without purification. Then, compound **3c** was prepared according to the synthesis method of **1b** on a 1 mmol scale. Purification by column chromatography afforded the title compound (112.1 mg, 39%). 1H NMR (400 MHz, DMSO- d_6) δ 11.18 (s, 1H), 7.66 (t, J = 7.8 Hz, 1H), 7.32 (d, J = 7.1 Hz, 1H), 7.26 (d, J = 8.4 Hz, 1H), 5.14 (dd, J = 13.0, 5.4 Hz, 1H), 2.99–2.87 (m, 1H), 2.76 (m,

1H), 2.57 (dd, $J = 13.0, 4.5$ Hz, 1H), 2.04 (m, 1H). HRMS m/z calculated for $C_{14}H_{13}N_2O_5$ [$M + H$]⁺: 289.0819, found: 289.0821.

4-[(7-Bromoheptyl)oxy]-2-(1-methyl-2,6-dioxopiperidin-3-yl)-2,3-dihydro-1H-isoindole-1,3-dione (3d). Compound 3d was prepared according to the general method to synthesize 1c–k on a 0.35 mmol scale of 3c (69.2 mg, 42%). ¹H NMR (400 MHz, chloroform-*d*) δ 7.59 (t, $J = 7.9$ Hz, 1H), 7.36 (d, $J = 7.3$ Hz, 1H), 7.14 (d, $J = 8.5$ Hz, 1H), 4.99–4.80 (m, 1H), 4.10 (t, $J = 6.5$ Hz, 2H), 3.34 (t, $J = 6.8$ Hz, 2H), 3.12 (s, 3H), 2.96–2.81 (m, 1H), 2.81–2.62 (m, 2H), 2.09–1.98 (m, 1H), 1.80 (m, $J = 6.5$ Hz, 4H), 1.39 (m, $J = 36.6, 15.1, 7.9$ Hz, 6H). HRMS m/z calculated for $C_{21}H_{26}BrN_2O_5$ [$M + H$]⁺: 465.1020, found: 465.1022.

N-[(4,6-Dimethyl-2-oxo-1,2-dihydropyridin-3-yl)methyl]-5-[ethyl(oxan-4-yl)amino]-4-methyl-4'-[[4-(7-[[2-(1-methyl-2,6-dioxopiperidin-3-yl)-1,3-dioxo-2,3-dihydro-1H-isoindol-4-yl]oxy]heptyl)piperazin-1-yl]methyl]-[1,1'-biphenyl]-3-carboxamide (E7-NC-1). E7-NC-1 was prepared according to the synthesis method of E7 on a 0.1 mmol scale of 3d (27.8 mg, 29%). ¹H NMR (400 MHz, CDCl₃) δ 11.68 (s, 1H), 7.66 (t, $J = 7.9$ Hz, 1H), 7.44 (d, $J = 7.6$ Hz, 3H), 7.34 (s, 1H), 7.32 (s, 2H), 7.28 (d, $J = 1.7$ Hz, 1H), 7.20 (d, $J = 8.4$ Hz, 1H), 7.15 (t, $J = 5.9$ Hz, 1H), 5.90 (s, 1H), 4.95 (dd, $J = 12.2, 5.4$ Hz, 1H), 4.55 (d, $J = 5.8$ Hz, 2H), 4.16 (t, $J = 6.6$ Hz, 2H), 3.94 (d, $J = 11.4$ Hz, 2H), 3.53 (s, 2H), 3.48 (s, 4H), 3.32 (m, $J = 11.2, 3.1$ Hz, 2H), 3.20 (s, 3H), 3.09 (q, $J = 7.0$ Hz, 2H), 2.99–2.94 (m, 1H), 2.83–2.70 (m, 1H), 2.51 (s, 6H), 2.40 (s, 3H), 2.34 (s, 4H), 2.13 (s, 3H), 1.87 (m, $J = 6.7$ Hz, 4H), 1.69 (d, $J = 10.5$ Hz, 4H), 1.50 (q, $J = 7.5$ Hz, 4H), 1.42–1.31 (m, 4H), 0.89 (t, $J = 6.9$ Hz, 3H). ¹³C NMR (101 MHz, CDCl₃) δ 166.5, 165.4, 164.0, 162.5, 161.1, 160.3, 151.9, 145.9, 144.7, 137.7, 134.6, 134.5, 133.6, 132.5, 131.7, 129.1, 128.5, 124.9, 122.0, 119.3, 117.4, 116.1, 114.1, 112.4, 110.9, 105.1, 64.7, 62.6, 57.9, 54.0, 53.7, 48.4, 48.2, 46.1, 45.1, 36.9, 31.4, 27.2, 25.8, 25.0, 24.5, 24.1, 22.7, 22.5, 21.9, 21.0, 17.2, 15.0, 14.0, 10.0, 8.1. HRMS m/z calculated for $C_{55}H_{70}N_7O_8$ [$M + H$]⁺: 956.5280, found: 956.5283.

tert-Butyl-4-[(3'-[ethyl(oxan-4-yl)amino]-4'-methyl-5'-[[1,4,6-trimethyl-2-oxo-1,2-dihydropyridin-3-yl)methyl]carbamoyl]-[1,1'-biphenyl]-4-yl)methyl]piperazine-1-carboxylate (3f). To a solution of 3e (120 mg, 0.25 mmol, 1 equiv), K₂CO₃ (69 mg, 0.5 mmol, 1 equiv) in DMF (2.5 mL) was added and stirred at 25 °C for 5 min before adding iodomethane (30 μ L). The mixture was stirred at 25 °C for 24 h and purified by column chromatography eluting to yield 3f (105.7 mg, 86%). ¹H NMR (400 MHz, DMSO-*d*₆) δ 8.17 (t, $J = 5.0$ Hz, 1H), 7.58 (d, $J = 7.9$ Hz, 2H), 7.43–7.32 (m, 3H), 7.21 (d, $J = 1.8$ Hz, 1H), 6.02 (s, 1H), 4.33 (d, $J = 5.0$ Hz, 2H), 3.83 (d, $J = 11.4$ Hz, 2H), 3.50 (s, 2H), 3.41 (s, 3H), 3.30 (s, 4H), 3.25 (t, $J = 11.5$ Hz, 2H), 3.09 (q, $J = 7.2$ Hz, 2H), 3.01 (d, $J = 11.1$ Hz, 1H), 2.33 (d, $J = 5.1$ Hz, 4H), 2.30 (s, 3H), 2.24 (s, 3H), 2.22 (s, 3H), 1.66 (d, $J = 12.5$ Hz, 2H), 1.52 (m, $J = 11.7, 9.9, 5.5$ Hz, 2H), 1.39 (s, 9H), 0.83 (t, $J = 6.9$ Hz, 3H). HRMS m/z calculated for $C_{40}H_{56}N_5O_5$ [$M + H$]⁺: 686.4276, found: 686.4279.

4'-[[4-(7-[[2-(2,6-Dioxopiperidin-3-yl)-1,3-dioxo-2,3-dihydro-1H-isoindol-4-yl]oxy]heptyl)piperazin-1-yl]methyl]-5-[ethyl(oxan-4-yl)amino]-4-methyl-N-[(1,4,6-trimethyl-2-oxo-1,2-dihydropyridin-3-yl)methyl]-[1,1'-biphenyl]-3-carboxamide (E7-NC-2). Compound E7-NC-2 was prepared according to the synthesis method of E7 on a 0.1 mmol scale of 3f (30.6 mg, 35%). ¹H NMR (400 MHz, chloroform-*d*) δ 7.66 (t, $J = 7.9$ Hz, 1H), 7.45 (dd, $J = 7.6, 5.0$ Hz, 3H), 7.38–7.29 (m, 3H), 7.26 (s, 1H), 7.20 (d, $J = 8.4$ Hz, 1H), 7.12 (t, $J = 6.1$ Hz, 1H), 5.99 (s, 1H), 4.92 (dd, $J = 11.9, 5.5$ Hz, 1H), 4.56 (d, $J = 6.1$ Hz, 2H), 4.18 (m, $J = 22.3, 14.4, 7.0$ Hz, 2H), 3.95 (d, 2H), 3.50 (s, 3H), 3.47 (s, 3H), 3.33 (m, $J = 11.6, 6.1$ Hz, 2H), 3.09 (q, $J = 6.9$ Hz, 2H), 3.01 (dd, $J = 10.6, 5.1$ Hz, 1H), 2.88–2.67 (m, 4H), 2.55 (s, 6H), 2.40 (s, 3H), 2.32 (s, 5H), 2.12 (m, 2H), 1.93–1.78 (m, 4H), 1.71 (s, 4H), 1.56–1.46 (m, 4H), 1.42 (d, 2H), 1.33 (d, $J = 4.8$ Hz, 2H), 0.90 (t, $J = 6.9$ Hz, 3H). ¹³C NMR (101 MHz, DMSO-*d*₆) δ 173.2, 170.8; 170.4, 169.5, 167.3, 165.8, 162.9, 156.5, 149.3, 147.8, 145.2, 140.0, 138.9, 137.9, 137.5, 133.7, 133.1, 129.9, 126.8, 123.3, 121.5, 121.3, 120.3, 116.7, 115.6, 109.0, 69.2, 66.8, 60.2, 58.3, 53.3, 53.1; 49.2, 41.6, 36.3, 31.4, 31.2, 30.8, 29.5, 29.0, 28.8, 27.3, 25.7, 22.5, 21.2, 20.5, 19.2, 15.0,

14.6, 13.2. HRMS m/z calculated for $C_{55}H_{70}N_7O_8$ [$M + H$]⁺: 956.5280, found: 956.5282.

Cell Lines and Culture. All of the cells used in this study were purchased from the American Type Culture Collection (ATCC, Manassas, VA) or the Cell Bank of the Chinese Academy of Science (Shanghai, China). Cells were cultured in Dulbecco's modified Eagle's medium (DMEM) or Rosewell Park Memorial Institute (RPMI) 1640 media containing 1% penicillin-streptomycin and 10% fetal bovine serum under humidified conditions with 5% CO₂ at 37 °C.

Biochemical Assay. The EZH1 and EZH2 inhibition assays were performed by the AlphaLISA immunodetection assay provided by Shanghai ChemPartner Limited (Shanghai, China). Values were determined using an AlphaLISA methyltransferase assay kit (PerkinElmer, MA) according to the manufacturer's protocol. The compounds' screening protocol is shown in the [Supporting Information](#).

Thermal Shift Assay. WSU-DLCL-2 cells were suspended at 1.5×10^6 cells/mL and pretreated with MG-132 for 1 h. E7 (60 μ M) was added, and cells were cultured for 2 h; an equal volume of DMSO served as the negative control. The cells were collected, and RIPA containing cocktail was added. After 1 h, the supernatant was collected by centrifugation and divided into six parts. The solutions were heated for 6 min at different temperatures (45, 48, 51, 54, 57, and 60 °C) and centrifuged at 13 000 rpm for 15 min. The supernatant solutions were used for immunoblotting analysis.

Immunoblotting Analysis. Protein samples were separated by sodium dodecyl sulphate-polyacrylamide gel electrophoresis (SDS-PAGE) and transferred to a nitrocellulose (NC) membrane. Then, the NC membrane was blocked with 5% skim milk for 2 h at room temperature, followed by incubation with the appropriate primary antibody at 4 °C overnight. The NC membrane was then incubated with the corresponding secondary antibody. Specific protein bands were obtained by chemiluminescence detection. The antibodies used for immunoblotting are listed in [Table S1](#).

Immunoprecipitation. Lysates were prepared from WSU-DLCL-2 cells treated with E7 for 48 h using the RIPA lysis buffer. The cell lysates were incubated with the indicated antibodies overnight at 4 °C, and then, Protein G agarose beads (Roche) were added. After 3 h incubation at 4 °C, the proteins were eluted from Protein G agarose beads with IP buffer, and ubiquitination modification of the target protein was examined by immunoblotting analysis.

Real-Time qPCR Assay. Cells were treated with different drugs for 48 h, and then, the total RNA was extracted with Trizol, according to the manufacturer's instruction. RNA was reverse-transcribed by Hiscript III RT SuperMix. RT-qPCR was carried out using the ChamQ Universal SYBR qPCR Master Mix on the CFX96 RT-qPCR system in accordance with the manufacturer's instruction. The reaction procedure was as follows: 95 °C for 30 s followed by 40 cycles of amplification for 6 s at 95 °C, 20 s at 60 °C. The primer sequences used for RT-qPCR are listed in [Table S2](#).

Cell Viability Assay. Cells were seeded ($1.5\text{--}8 \times 10^3$ cells per well in 100 μ L of medium) in 96-well plates for 24 h. Then, 100 μ L of medium containing various concentrations of E7 was added to each well. After the indicated incubation time, 20 μ L of a 5 mg/mL 3-(4,5-dimethylthiazol-2-yl)-2,5-diphenyltetrazolium bromide (MTT) solution was added to each well and cells were incubated for an additional 2.5 h at 37 °C. For A549 and NCI-H1299 cells, the medium was removed; 150 μ L of DMSO was added to each well, and then, the absorbance of each well was measured at 570 nm. For WSU-DLCL-2 and Pfeiffer cells, 50 μ L of 20% (w/v) SDS was directly added to each well and cells were incubated at 37 °C overnight; the absorbance of each well was measured at 570 nm wavelength.

Cell Proliferation Analysis. Cells were seeded in 12-well plates (5×10^3 cells per well), incubated for 24 h, and treated with 10 μ M E7, EPZ6438, or GSK126 for 9 days. The cells were photographed and counted on days 1, 3, 5, 7, and 9, and the medium was refreshed.

Statistical Analysis. All quantitative results were expressed as mean values \pm SD. Statistically significant differences were obtained via Student's *t*-test. $P < 0.05$ can be considered statistically significant.

■ ASSOCIATED CONTENT

Supporting Information

The Supporting Information is available free of charge at <https://pubs.acs.org/doi/10.1021/acs.jmedchem.0c02234>.

Protein levels of PRC2 subunits and H3K27me3 in WSU-DLCL-2 cells treated with indicated compounds for 48 h analyzed by western blot; potencies of E7 against WSU-DLCL-2, A549, NCI-H1299, and Pfeiffer cancer cell lines; compounds' screening methods against EZH1 and EZH2; EZH1 inhibitory activities of the synthesized compounds; transfection of EZH2-shRNA and siRNA; antibodies used in immunoblotting analysis; primer sequences used in RT-qPCR; ¹H NMR, ¹³C NMR, and HRMS spectrogram data of all target compounds including G4–G12, E4–E12, E7-NC-1, and E7-NC-2; and HPLC for purity determination of E7 (PDF)

Molecular formula strings (CSV)

■ AUTHOR INFORMATION

Corresponding Authors

Ningyu Wang – School of Life Science and Engineering, Southwest Jiaotong University, Chengdu 610031, China; orcid.org/0000-0003-3571-4903; Email: wangny-swjtu@swjtu.edu.cn

Luoting Yu – State Key Laboratory of Biotherapy and Cancer Center, West China Hospital, and Collaborative Innovation Center of Biotherapy, Sichuan University, Chengdu 610041, China; orcid.org/0000-0001-9297-6665; Email: yuluot@scu.edu.cn

Authors

Zhihao Liu – State Key Laboratory of Biotherapy and Cancer Center, West China Hospital, and Collaborative Innovation Center of Biotherapy, Sichuan University, Chengdu 610041, China; orcid.org/0000-0002-0246-8761

Xi Hu – State Key Laboratory of Biotherapy and Cancer Center, West China Hospital, and Collaborative Innovation Center of Biotherapy, Sichuan University, Chengdu 610041, China

Qiwei Wang – State Key Laboratory of Biotherapy and Cancer Center, West China Hospital, and Collaborative Innovation Center of Biotherapy, Sichuan University, Chengdu 610041, China

Xiuli Wu – State Key Laboratory of Biotherapy and Cancer Center, West China Hospital, and Collaborative Innovation Center of Biotherapy, Sichuan University, Chengdu 610041, China

Qiangsheng Zhang – State Key Laboratory of Biotherapy and Cancer Center, West China Hospital, and Collaborative Innovation Center of Biotherapy, Sichuan University, Chengdu 610041, China

Wei Wei – State Key Laboratory of Biotherapy and Cancer Center, West China Hospital, and Collaborative Innovation Center of Biotherapy, Sichuan University, Chengdu 610041, China

Xingping Su – State Key Laboratory of Biotherapy and Cancer Center, West China Hospital, and Collaborative Innovation Center of Biotherapy, Sichuan University, Chengdu 610041, China

Hualong He – State Key Laboratory of Biotherapy and Cancer Center, West China Hospital, and Collaborative

Innovation Center of Biotherapy, Sichuan University, Chengdu 610041, China

Shuyan Zhou – State Key Laboratory of Biotherapy and Cancer Center, West China Hospital, and Collaborative Innovation Center of Biotherapy, Sichuan University, Chengdu 610041, China

Rong Hu – School of Life Science and Engineering, Southwest Jiaotong University, Chengdu 610031, China

Tinghong Ye – State Key Laboratory of Biotherapy and Cancer Center, West China Hospital, and Collaborative Innovation Center of Biotherapy, Sichuan University, Chengdu 610041, China

Yongxia Zhu – Department of Pharmacy, Sichuan Cancer Hospital & Institute, Sichuan Cancer Center, School of Medicine, University of Electronic Science and Technology of China, Chengdu 610041, China

Complete contact information is available at:

<https://pubs.acs.org/doi/10.1021/acs.jmedchem.0c02234>

Author Contributions

^{||}Z.L. and X.H. contributed equally to this work.

Notes

The authors declare no competing financial interest.

■ ACKNOWLEDGMENTS

We are grateful to Guobo Li of West China School of Pharmacy (Sichuan University) for advice on the PROTAC molecule design, Shuhui Xu of State Key Laboratory of Biotherapy (Sichuan University) for NMR measurements, and Professor Lijuan Chen's team of State Key Laboratory of Biotherapy (Sichuan University) for HRMS measurements. This work was supported by grants from the Sichuan Provincial Science and Technology Program for Key Research and Development, China (No. 2018SZ0007), the Postdoctoral Science Foundation of Sichuan University (No. 2020SCU12020), the National Natural Science Foundation of China (No. 81702946), and the National S&T Major Special Project on Major New Drug Innovations (No. 2018ZX09201018).

■ ABBREVIATIONS

PRC2, polycomb repressive complex 2; H3K27me3, histone 3 lysine 27 trimethyl; EZH2, enhancer of zeste homolog 2; EED, embryonic ectoderm development; SUZ12, suppressor of zeste 12 protein homolog; RbAp46/48, retinoblastoma (Rb)-associated proteins 46/48; SAM, S-adenosyl-L-methionine; GCB, germinal center B-cell; DLBCL, diffuse large-cell B-cell lymphomas; NHL, non-Hodgkin's lymphomas; SWI/SNF, switch/sucrose nonfermentable; A, alanine; Y, tyrosine; F, phenylalanine; N, asparagine; S, serine; C, cystine; H, histidine; AR, androgen receptor; SWI/SNF, switch/sucrose nonfermentable; HyT, hydrophobic tagging; PROTACS, proteolysis targeting chimeras; POI, protein of interest; CRBN, cereblon; DMSO, dimethyl sulfoxide; Boc, tert-butylloxycarbonyl; MTT, 3-(4,5-dimethylthiazol-2-yl)-2,5-diphenyltetrazolium bromide; RT-qPCR, quantitative real-time polymerase chain reaction; WB, western blot; IP, immunoprecipitation

■ REFERENCES

(1) Margueron, R.; Reinberg, D. The polycomb complex PRC2 and its mark in life. *Nature* **2011**, *469*, 343–349.

- (2) Deevy, O.; Bracken, A. P. PRC2 functions in development and congenital disorders. *Development* **2019**, *146*, No. dev181354.
- (3) Cao, R.; Wang, L.; Wang, H.; Xia, L.; Erdjument-Bromage, H.; Tempst, P.; Jones, R. S.; Zhang, Y. Role of histone H3 lysine 27 methylation in polycomb-group silencing. *Science* **2002**, *298*, 1039–1043.
- (4) Müller, J.; Hart, C. M.; Francis, N. J.; Vargas, M. L.; Sengupta, A.; Wild, B.; Müller, E. L.; O'Connor, M. B.; Kingston, R. E.; Simon, J. A. Histone methyltransferase activity of a drosophila polycomb group repressor complex. *Cell* **2002**, *111*, 197–208.
- (5) Czermin, B.; Melfi, R.; McCabe, D.; Seitz, V.; Imhof, A.; Pirrotta, V. Drosophila enhancer of zeste/ESC Complexes have a histone H3 methyltransferase activity that marks chromosomal polycomb sites. *Cell* **2002**, *111*, 185–196.
- (6) Kim, K. H.; Roberts, C. W. Targeting EZH2 in cancer. *Nat. Med.* **2016**, *22*, 128–134.
- (7) Varambally, S.; Dhanasekaran, S. M.; Zhou, M.; Barrette, T. R.; Kumar-Sinha, C.; Sanda, M. G.; Ghosh, D.; Pienta, K. J.; Sewalt, R. G.; Otte, A. P.; Rubin, M. A.; Chinnaiyan, A. M. The polycomb group protein EZH2 is involved in progression of prostate cancer. *Nature* **2002**, *419*, 624–629.
- (8) Cao, Q.; Yu, J.; Dhanasekaran, S. M.; Kim, J. H.; Mani, R. S.; Tomlins, S. A.; Mehra, R.; Laxman, B.; Cao, X.; Yu, J.; Kleer, C. G.; Varambally, S.; Chinnaiyan, A. M. Repression of E-cadherin by the polycomb group protein EZH2 in cancer. *Oncogene* **2008**, *27*, 7274–7284.
- (9) Yang, X.; Karuturi, R. K.; Sun, F.; Aau, M.; Yu, K.; Shao, R.; Miller, L. D.; Tan, P. B.; Yu, Q. CDKN1C (p57) is a direct target of EZH2 and suppressed by multiple epigenetic mechanisms in breast cancer cells. *PLoS One* **2009**, *4*, No. e5011.
- (10) Taniguchi, H.; Jacinto, F. V.; Villanueva, A.; Fernandez, A. F.; Yamamoto, H.; Carmona, F. J.; Puertas, S.; Marquez, V. E.; Shinomura, Y.; Imai, K.; Esteller, M. Silencing of kruppel-like factor 2 by the histone methyltransferase EZH2 in human cancer. *Oncogene* **2012**, *31*, 1988–1994.
- (11) Chang, C. J.; Yang, J. Y.; Xia, W.; Chen, C. T.; Xie, X.; Chao, C. H.; Woodward, W. A.; Hsu, J. M.; Hortobagyi, G. N.; Hung, M. C. EZH2 promotes expansion of breast tumor initiating cells through activation of RAF1-beta-catenin signaling. *Cancer Cell* **2011**, *19*, 86–100.
- (12) Lu, C.; Han, H. D.; Mangala, L. S.; Ali-Fehmi, R.; Newton, C. S.; Ozburn, L.; Armaiz-Pena, G. N.; Hu, W.; Stone, R. L.; Munkarah, A.; Ravoori, M. K.; Shahzad, M. M.; Lee, J. W.; Mora, E.; Langley, R. R.; Carroll, A. R.; Matsuo, K.; Spannuth, W. A.; Schmandt, R.; Jennings, N. B.; Goodman, B. W.; Jaffe, R. B.; Nick, A. M.; Kim, H. S.; Guven, E. O.; Chen, Y. H.; Li, L. Y.; Hsu, M. C.; Coleman, R. L.; Calin, G. A.; Denkbass, E. B.; Lim, J. Y.; Lee, J. S.; Kundra, V.; Birrer, M. J.; Hung, M. C.; Lopez-Berestein, G.; Sood, A. K. Regulation of tumor angiogenesis by EZH2. *Cancer Cell* **2010**, *18*, 185–197.
- (13) Jones, B. A.; Varambally, S.; Arend, R. C. Histone methyltransferase EZH2: a therapeutic target for ovarian cancer. *Mol. Cancer Ther.* **2018**, *17*, 591–602.
- (14) Hussain, M.; Rao, M.; Humphries, A. E.; Hong, J. A.; Liu, F.; Yang, M.; Caragacianu, D.; Schrupp, D. S. Tobacco smoke induces polycomb-mediated repression of Dickkopf-1 in lung cancer cells. *Cancer Res.* **2009**, *69*, 3570–3578.
- (15) Morin, R. D.; Johnson, N. A.; Severson, T. M.; Mungall, A. J.; An, J.; Goya, R.; Paul, J. E.; Boyle, M.; Woolcock, B. W.; Kuchenbauer, F.; Yap, D.; Humphries, R. K.; Griffith, O. L.; Shah, S.; Zhu, H.; Kimbara, M.; Shashkin, P.; Charlot, J. F.; Tcherpakov, M.; Corbett, R.; Tam, A.; Varhol, R.; Smailus, D.; Moksa, M.; Zhao, Y.; Delaney, A.; Qian, H.; Birol, I.; Schein, J.; Moore, R.; Holt, R.; Horsman, D. E.; Connors, J. M.; Jones, S.; Aparicio, S.; Hirst, M.; Gascogne, R. D.; Marra, M. A. Somatic mutations altering EZH2 (Tyr641) in follicular and diffuse large B-cell lymphomas of germinal-center origin. *Nat. Genet.* **2010**, *42*, 181–185.
- (16) Baumgart, S.; Ellenrieder, V.; Fernandez-Zapico, M. E. Oncogenic transcription factors: cornerstones of inflammation-linked pancreatic carcinogenesis. *Gut* **2013**, *62*, 310–316.
- (17) Bödör, C.; O'Riain, C.; Wrench, D.; Matthews, J.; Iyengar, S.; Tayyib, H.; Calaminici, M.; Clear, A.; Iqbal, S.; Quentmeier, H.; Drexler, H. G.; Montoto, S.; Lister, A. T.; Gribben, J. G.; Matolcsy, A.; Fitzgibbon, J. EZH2 Y641 mutations in follicular lymphoma. *Leukemia* **2011**, *25*, 726–729.
- (18) Majer, C. R.; Jin, L.; Scott, M. P.; Knutson, S. K.; Kuntz, K. W.; Keilhack, H.; Smith, J. J.; Moyer, M. P.; Richon, V. M.; Copeland, R. A.; Wigle, T. J. A687V EZH2 is a gain-of-function mutation found in lymphoma patients. *FEBS Lett.* **2012**, *586*, 3448–3451.
- (19) McCabe, M. T.; Graves, A. P.; Ganji, G.; Diaz, E.; Halsey, W. S.; Jiang, Y.; Smitheman, K. N.; Ott, H. M.; Pappalardi, M. B.; Allen, K. E.; Chen, S. B.; Della Pietra, A., 3rd; Dul, E.; Hughes, A. M.; Gilbert, S. A.; Thrall, S. H.; Tummino, P. J.; Kruger, R. G.; Brandt, M.; Schwartz, B.; Creasy, C. L. Mutation of A677 in histone methyltransferase EZH2 in human B-cell lymphoma promotes hypertrimethylation of histone H3 on lysine 27 (H3K27). *Proc. Natl. Acad. Sci. U.S.A.* **2012**, *109*, 2989–2994.
- (20) McCabe, M. T.; Ott, H. M.; Ganji, G.; Korenchuk, S.; Thompson, C.; Van Aller, G. S.; Liu, Y.; Graves, A. P.; Della Pietra, A., 3rd; Diaz, E.; LaFrance, L. V.; Mellinger, M.; Duquenne, C.; Tian, X.; Kruger, R. G.; McHugh, C. F.; Brandt, M.; Miller, W. H.; Dhanak, D.; Verma, S. K.; Tummino, P. J.; Creasy, C. L. EZH2 inhibition as a therapeutic strategy for lymphoma with EZH2-activating mutations. *Nature* **2012**, *492*, 108–112.
- (21) Knutson, S. K.; Wigle, T. J.; Warholik, N. M.; Sneeringer, C. J.; Allain, C. J.; Klaus, C. R.; Sacks, J. D.; Raimondi, A.; Majer, C. R.; Song, J.; Scott, M. P.; Jin, L.; Smith, J. J.; Olhava, E. J.; Chesworth, R.; Moyer, M. P.; Richon, V. M.; Copeland, R. A.; Keilhack, H.; Pollock, R. M.; Kuntz, K. W. A selective inhibitor of EZH2 blocks H3K27 methylation and kills mutant lymphoma cells. *Nat. Chem. Biol.* **2012**, *8*, 890–896.
- (22) Knutson, S. K.; Warholik, N. M.; Wigle, T. J.; Klaus, C. R.; Allain, C. J.; Raimondi, A.; Porter Scott, M.; Chesworth, R.; Moyer, M. P.; Copeland, R. A.; Richon, V. M.; Pollock, R. M.; Kuntz, K. W.; Keilhack, H. Durable tumor regression in genetically altered malignant rhabdoid tumors by inhibition of methyltransferase EZH2. *Proc. Natl. Acad. Sci. U.S.A.* **2013**, *110*, 7922–7927.
- (23) Kung, P. P.; Bingham, P.; Brooun, A.; Collins, M.; Deng, Y. L.; Dinh, D.; Fan, C.; Gajiwala, K. S.; Grantner, R.; Gukasyan, H. J.; Hu, W.; Huang, B.; Kania, R.; Kephart, S. E.; Krivacic, C.; Kumpf, R. A.; Khamphavong, P.; Kraus, M.; Liu, W.; Maegley, K. A.; Nguyen, L.; Ren, S.; Richter, D.; Rollins, R. A.; Sach, N.; Sharma, S.; Sherrill, J.; Spangler, J.; Stewart, A. E.; Sutton, S.; Uryu, S.; Verhelle, D.; Wang, H.; Wang, S.; Wythes, M.; Xin, S.; Yamazaki, S.; Zhu, H.; Zhu, J.; Zehnder, L.; Edwards, M. Optimization of orally bioavailable enhancer of zeste homolog 2 (EZH2) inhibitors using ligand and property-based design strategies: identification of development candidate (R)-5,8-Dichloro-7-(methoxy(oxetan-3-yl)methyl)-2-((4-methoxy-6-methyl-2-oxo-1,2-dihydropyridin-3-yl)methyl)-3,4-dihydroisoquinolin-1(2H)-one (PF-06821497). *J. Med. Chem.* **2018**, *61*, 650–665.
- (24) Vaswani, R. G.; Gehling, V. S.; Dakin, L. A.; Cook, A. S.; Nasveschuk, C. G.; Duplessis, M.; Iyer, P.; Balasubramanian, S.; Zhao, F.; Good, A. C.; Campbell, R.; Lee, C.; Cantone, N.; Cummings, R. T.; Normant, E.; Bellon, S. F.; Albrecht, B. K.; Harmange, J. C.; Trojer, P.; Audia, J. E.; Zhang, Y.; Justin, N.; Chen, S.; Wilson, J. R.; Gamblin, S. J. Identification of (R)-N-((4-Methoxy-6-methyl-2-oxo-1,2-dihydropyridin-3-yl)methyl)-2-methyl-1-(1-(1-(2,2,2-trifluoroethyl)piperidin-4-yl)ethyl)-1H-indole-3-carboxamide (CPI-1205), a potent and selective inhibitor of histone methyltransferase EZH2, suitable for phase I clinical trials for B-cell lymphomas. *J. Med. Chem.* **2016**, *59*, 9928–9941.
- (25) Epizyme Announces U.S. FDA Accelerated Approval of TAZVERIK (tazemetostat) for the Treatment of Patients with Epithelioid Sarcoma. <https://epizyme.gcs-web.com/news-releases/news-release-details/epizyme-announces-us-fda-accelerated-approval-tazveriktm> (accessed Jan 23, 2020).
- (26) Huang, X.; Yan, J.; Zhang, M.; Wang, Y.; Chen, Y.; Fu, X.; Wei, R.; Zheng, X. L.; Liu, Z.; Zhang, X.; Yang, H.; Hao, B.; Shen, Y. Y.; Su,

Y.; Cong, X.; Huang, M.; Tan, M.; Ding, J.; Geng, M. Targeting epigenetic crosstalk as a therapeutic strategy for EZH2-aberrant solid tumors. *Cell* **2018**, *175*, 186.e19–199.e19.

(27) Shi, B.; Liang, J.; Yang, X.; Wang, Y.; Zhao, Y.; Wu, H.; Sun, L.; Zhang, Y.; Chen, Y.; Li, R.; Zhang, Y.; Hong, M.; Shang, Y. Integration of estrogen and Wnt signaling circuits by the polycomb group protein EZH2 in breast cancer cells. *Mol. Cell. Biol.* **2007**, *27*, 5105–5119.

(28) Jung, H. Y.; Jun, S.; Lee, M.; Kim, H. C.; Wang, X.; Ji, H.; McCrea, P. D.; Park, J. I. PAF and EZH2 induce Wnt/beta-catenin signaling hyperactivation. *Mol. Cell* **2013**, *52*, 193–205.

(29) Gonzalez, M. E.; Moore, H. M.; Li, X.; Toy, K. A.; Huang, W.; Sabel, M. S.; Kidwell, K. M.; Kleer, C. G. EZH2 expands breast stem cells through activation of NOTCH1 signaling. *Proc. Natl. Acad. Sci. U.S.A.* **2014**, *111*, 3098–3103.

(30) Lee, S. T.; Li, Z.; Wu, Z.; Aau, M.; Guan, P.; Karuturi, R. K.; Liou, Y. C.; Yu, Q. Context-specific regulation of NF-kappaB target gene expression by EZH2 in breast cancers. *Mol. Cell* **2011**, *43*, 798–810.

(31) Xu, K.; Wu, Z. J.; Groner, A. C.; He, H. H.; Cai, C.; Lis, R. T.; Wu, X.; Stack, E. C.; Loda, M.; Liu, T.; Xu, H.; Cato, L.; Thornton, J. E.; Gregory, R. I.; Morrissey, C.; Vessella, R. L.; Montironi, R.; Magi-Galluzzi, C.; Kantoff, P. W.; Balk, S. P.; Liu, X. S.; Brown, M. EZH2 oncogenic activity in castration-resistant prostate cancer cells is Polycomb-independent. *Science* **2012**, *338*, 1465–1469.

(32) Cavalli, G. Molecular biology. EZH2 goes solo. *Science* **2012**, *338*, 1430–1431.

(33) Kim, K. H.; Kim, W.; Howard, T. P.; Vazquez, F.; Tsherniak, A.; Wu, J. N.; Wang, W.; Haswell, J. R.; Walensky, L. D.; Hahn, W. C.; Orkin, S. H.; Roberts, C. W. SWI/SNF-mutant cancers depend on catalytic and non-catalytic activity of EZH2. *Nat. Med.* **2015**, *21*, 1491–1496.

(34) Lai, A. C.; Crews, C. M. Induced protein degradation: an emerging drug discovery paradigm. *Nat. Rev. Drug Discovery* **2017**, *16*, 101–114.

(35) Neklesa, T. K.; Tae, H. S.; Schneekloth, A. R.; Stulberg, M. J.; Corson, T. W.; Sundberg, T. B.; Raina, K.; Holley, S. A.; Crews, C. M. Small-molecule hydrophobic tagging-induced degradation of HaloTag fusion proteins. *Nat. Chem. Biol.* **2011**, *7*, 538–543.

(36) Ma, A.; Stratikopoulos, E.; Park, K. S.; Wei, J.; Martin, T. C.; Yang, X.; Schwarz, M.; Leshchenko, V.; Rialdi, A.; Dale, B.; Lagana, A.; Guccione, E.; Parekh, S.; Parsons, R.; Jin, J. Discovery of a first-in-class EZH2 selective degrader. *Nat. Chem. Biol.* **2019**, *16*, 214–222.

(37) Salami, J.; Crews, C. M. Waste disposal—an attractive strategy for cancer therapy. *Science* **2017**, *355*, 1163–1167.

(38) Burslem, G. M.; Crews, C. M. Small-molecule modulation of protein homeostasis. *Chem. Rev.* **2017**, *117*, 11269–11301.

(39) Churcher, I. Protac-induced protein degradation in drug discovery: breaking the rules or just making new ones? *J. Med. Chem.* **2018**, *61*, 444–452.

(40) Hsu, J. H.; Rasmusson, T.; Robinson, J.; Pacht, F.; Read, J.; Kawatkar, S.; DH, O. D.; Bagal, S.; Code, E.; Rawlins, P.; Argyrou, A.; Tomlinson, R.; Gao, N.; Zhu, X.; Chiarparin, E.; Jacques, K.; Shen, M.; Woods, H.; Bednarski, E.; Wilson, D. M.; Drew, L.; Castaldi, M. P.; Fawell, S.; Bloecher, A. EED-targeted PROTACs degrade EED, EZH2, and SUZ12 in the PRC2 complex. *Cell Chem. Biol.* **2020**, *27*, 41–46 e17.

(41) Potjewyd, F.; Turner, A. W.; Beri, J.; Rectenwald, J. M.; Norris-Drouin, J. L.; Cholensky, S. H.; Margolis, D. M.; Pearce, K. H.; Herring, L. E.; James, L. I. Degradation of polycomb repressive complex 2 with an EED-targeted bivalent chemical degrader. *Cell Chem. Biol.* **2020**, *27*, 47.e15–56.e15.

(42) Winter, G. E.; Buckley, D. L.; Paulk, J.; Roberts, J. M.; Souza, A.; Dhe-Paganon, S.; Bradner, J. E. DRUG DEVELOPMENT. Phthalimide conjugation as a strategy for in vivo target protein degradation. *Science* **2015**, *348*, 1376–1381.

(43) Smith, B. E.; Wang, S. L.; Jaime-Figueroa, S.; Harbin, A.; Wang, J.; Hamman, B. D.; Crews, C. M. Differential PROTAC substrate

specificity dictated by orientation of recruited E3 ligase. *Nat. Commun.* **2019**, *10*, No. 131.

(44) Lai, A. C.; Toure, M.; Hellerschmied, D.; Salami, J.; Jaime-Figueroa, S.; Ko, E.; Hines, J.; Crews, C. M. Modular PROTAC design for the degradation of oncogenic BCR-ABL. *Angew. Chem., Int. Ed.* **2016**, *55*, 807–810.

(45) Su, S.; Yang, Z.; Gao, H.; Yang, H.; Zhu, S.; An, Z.; Wang, J.; Li, Q.; Chandarlapaty, S.; Deng, H.; Wu, W.; Rao, Y. Potent and preferential degradation of CDK6 via proteolysis targeting chimera degraders. *J. Med. Chem.* **2019**, *62*, 7575–7582.

(46) Bratkowski, M.; Yang, X.; Liu, X. An evolutionarily conserved structural platform for PRC2 inhibition by a class of EZH2 inhibitors. *Sci. Rep.* **2018**, *8*, No. 9092.

(47) Nowak, R. P.; DeAngelo, S. L.; Buckley, D.; He, Z.; Donovan, K. A.; An, J.; Safaei, N.; Jedrychowski, M. P.; Ponthier, C. M.; Ishoey, M.; Zhang, T.; Mancias, J. D.; Gray, N. S.; Bradner, J. E.; Fischer, E. S. Plasticity in binding confers selectivity in ligand-induced protein degradation. *Nat. Chem. Biol.* **2018**, *14*, 706–714.

(48) Martinez Molina, D.; Jafari, R.; Ignatshchenko, M.; Seki, T.; Larsson, E. A.; Dan, C.; Sreekumar, L.; Cao, Y.; Nordlund, P. Monitoring drug target engagement in cells and tissues using the cellular thermal shift assay. *Science* **2013**, *341*, 84–87.

(49) Toure, M.; Crews, C. M. Small-molecule PROTACS: new approaches to protein degradation. *Angew. Chem., Int. Ed.* **2016**, *55*, 1966–1973.

(50) Leeb, M.; Pasini, D.; Novatchkova, M.; Jaritz, M.; Helin, K.; Wutz, A. Polycomb complexes act redundantly to repress genomic repeats and genes. *Genes Dev.* **2010**, *24*, 265–276.

(51) Xu, J.; Shao, Z.; Li, D.; Xie, H.; Kim, W.; Huang, J.; Taylor, J. E.; Pinello, L.; Glass, K.; Jaffe, J. D.; Yuan, G. C.; Orkin, S. H. Developmental control of polycomb subunit composition by GATA factors mediates a switch to non-canonical functions. *Mol. Cell* **2015**, *57*, 304–316.

(52) Zhang, K. L.; Shen, Q. Q.; Fang, Y. F.; Sun, Y. M.; Ding, J.; Chen, Y. AZD9291 inactivates the PRC2 complex to mediate tumor growth inhibition. *Acta Pharmacol. Sin.* **2019**, *40*, 1587–1595.

NOTE ADDED AFTER ASAP PUBLICATION

Due to a production error, the version of this paper that was published ASAP February 19, 2021, was missing “PRC2” in the title. The corrected version was reposted February 22, 2021.